Heliyon 10 (2024) e34554

Contents lists available at ScienceDirect

Heliyon

journal homepage: www.cell.com/heliyon

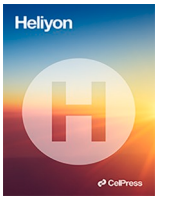

Research article

Chitosan-coated liposomal systems for delivery of antibacterial peptide LL17-32 to *Porphyromonas gingivalis*

Jinyang Han [a], Josephine Meade [b], Deirdre Devine [b], Amin Sadeghpour [a], Michael Rappolt [a], Francisco M. Goycoolea [a,c,*]

[a] School of Food Science and Nutrition, University of Leeds, Woodhouse Ln, Leeds, LS2 9JT, United Kingdom
[b] School of Dentistry, University of Leeds, Woodhouse Ln, Leeds, LS2 9JT, United Kingdom
[c] Department of Cell Biology and Histology, University of Murcia, Campus de Espinardo, Murcia, 30100, Spain

ARTICLE INFO

Keywords:
Antimicrobial peptide
LL37
LL17-32
Liposome
Porphyromonas gingivalis
Chitosan
Nanomaterials
Periodontal disease
Human cathelicidin
SAXS

ABSTRACT

Periodontal disease is triggered by surface bacterial biofilms where bacteria are less susceptible to antibiotic treatment. The development of liposome-based delivery mechanisms for the therapeutic use of antimicrobial peptides is an attractive alternative in this regard. The cationic antimicrobial peptide LL-37 (human cathelicidin) is well-known to exert antibacterial activity against *Porphyromonas gingivalis,* a keystone oral pathogen. However, the antibacterial activity of the 16-amino acid fragment (LL17-32) of LL-37, is unknown. In addition, there are still gaps in studies using liposomal formulations as delivery vehicles of antibacterial peptides against this pathogen. This study was designed to examine the influence of the different types of liposomal formulations to associate and deliver LL17-32 to act against *P. gingivalis*. Chitosans of varying Mw and degree of acetylation (DA) were adsorbed at the surface of soya lecithin (SL) liposomes. Their bulk (average hydrodynamic size, ζ-potential and membrane fluidity) and ultrastructural (*d*-spacing, half-bilayer thickness and the water layer thickness) biophysical properties were investigated by a panel of techniques (DLS, SAXS, M3-PALS, fluorescence spectroscopy and TEM imaging). Their association efficiency, *in vitro* release, stability, and efficacy in killing the periodontal pathogen *P. gingivalis* were also investigated. All liposomal systems possessed spherical morphologies and good shelf-life stabilities. Under physiological conditions, chitosan formulations with a high DA demonstrated enhanced stability in comparison to low DA-chitosan formulations. Chitosans and LL17-32 both decreased SL-liposomal membrane fluidity. LL17-32 exhibited a high degree of association with SL-liposomes without *in vitro* release. In biological studies, free LL17-32 or chitosans alone, demonstrated microbicidal activity against *P. gingivalis*, however this was attenuated when LL17-32 was loaded onto the SL-liposome delivery system, presumably due to the restrained release of the peptide. A property that could be harnessed in future studies (*e.g.*, oral mucoadhesive slow-release formulations).

1. Introduction

Periodontal diseases (PD) are prevalent oral cavity biofilm-mediated diseases, affecting 10–15 % of adult populations worldwide

* Corresponding author. School of Food Science and Nutrition, University of Leeds, Woodhouse Ln, Leeds, LS2 9JT, United Kingdom
E-mail address: F.M.Goycoolea@leeds.ac.uk (F.M. Goycoolea).

https://doi.org/10.1016/j.heliyon.2024.e34554
Received 18 February 2024; Received in revised form 29 May 2024; Accepted 11 July 2024
Available online 14 July 2024

[1]. In developing countries, the incidence of PD can be as high as 70 % of the population [2]. *Porphyromonas gingivalis*, an anaerobic, Gram-negative rod, is a keystone pathogenic bacterium contributing to the onset and progression of periodontitis [3]. The concept of keystone pathogens is one where their effects have community-wide significance that is disproportionate to their abundance. *P. gingivalis* produces a repertoire of virulence factors including fimbriae, a capsule, lipopolysaccharide, proteases, and outer membrane proteins. Through the action of these virulence factors, *P. gingivalis* is able to disrupt homeostasis between the host and the commensal microbiota and can promote changes in the composition of the bacterial community favouring disease associated species known as dysbiosis. These factors can also manipulate both the innate and adaptive arms of the host immune response and all of these actions drive increased subgingival microbial growth, inflammation and subsequent destruction of oral tissues [4–6]. *P. gingivalis* has been reported to be associated with serious systemic conditions most likely through shared inflammatory aetiologies, including cardiovascular disease, rheumatoid arthritis, metabolic diseases, pancreatic cancer and Alzheimer's disease [7–11].

Many approaches to preventing or treating PD have been researched, including developing novel potential therapeutics against oral bacteria and/or oral biofilms. Antimicrobial peptides (AMPs), one category of therapeutic candidates, are currently presented as promising alternatives to antibiotics, as they have a broad spectrum of activity against pathogenic microorganisms and a relatively low tendency for developing resistant strains. More than 3000 AMPs have been discovered in bacteria, insects, amphibians, fish, plants, fungi, viruses, protozoa and mammals with different modes of action against both Gram-positive and Gram-negative bacteria [12,13]. Some AMPs show high antibacterial activity *in vitro*; however, there are some undesirable characteristics for clinical use. These include undesirable effects on eukaryotic cells such as neurotoxicity, haemolysis, and nephrotoxicity. AMPs can also be susceptible to degradation by bacterial proteases [14,15] and their pharmacokinetic profile is not well understood [16]. To mitigate for some of the limiting aspects, liposomes and polymeric nanoparticle vehicles have been reported to reduce cytotoxicity, provide sustained release and improve bactericidal effect of AMPs. However, this is an area which still is in early stages of development.

LL17-32, an active segment of the known LL-37 peptide (cathelicidin antimicrobial peptide, CAMP), was chosen in this study. The primary structure of LL17-32, FKRIVQRIKDFLRNLV, was obtained by removing non-antimicrobial activity residues from CAMP, namely 1–12, nonessential micelle-binding residues, 13–16 and 33–37 residues. Antibacterial and anticancer assays found that LL17-32 was more active than LL-37 and other α-helical CAMP-derived AMPs such as LL13-37, LL1-4, LL17-27, and LL17-29 [17]. Also, studies showed that N-terminal fragments 1–12 and 1–20 presented no activity on antibacterial, anticancer, and haemolytic effects [17,18]. The combination of the biological and computational approach with experimental biophysical techniques (conventional and surface-enhanced IR absorption (SEIRA) spectroscopy) suggested that fragment LL1-20 is unable to intercalate to the membrane surface or into the membrane interior [18]. In spite of the presence of seven positively charged amino acids and three negatively charged amino acids in LL-20, the distance between oppositely charged amino acid chains enable them to form salt bridges. As a result, most charges are compensated for each other. Salt bridges also bring rigidity to the peptide, which decreases the flexibility of the backbone and impairs flexible cationic side chains from interacting with anionic membrane surfaces. Additionally, a flexible site was predicted at positions R19−R23, which are involved in the active core of LL-37. Depending on its structural flexibility, this region may confer versatility to the polypeptide chain, which is critical to the efficient penetration of lipid bilayers [18]. The sequence of peptide LL17-32 (FKRIVQRIKDFLRNLV) used in this work reveals a highly charged nature and both hydrophobic and hydrophilic surface amino acids. Such a structural feature is ideal for targeting negatively charged bacterial membranes [17].

Liposomes, originally discovered in the 1960s, are a well-established drug/bioactives delivery platform for cosmetic, food and pharmaceutical industries, and have been approved as drug delivery vehicles since the mid-nineties [19]. They can encapsulate bioactive compounds either in their aqueous core or in the lipid bilayer, depending on their inherent hydrophilicity or hydrophobicity. Due to their bilayer of amphiphilic phospholipidic character, which is similar to mammalian plasma membranes, liposomes can interact effectively with cell membranes and facilitate cellular uptake, resulting in high intracellular concentrations and reduced toxicity and improving the therapeutic effect [20,21]. As a result of their non-toxicity, non-immunogenic biodegradability, biocompatibility, small size and both lipophilic and hydrophilic characteristics, liposomes account for a large proportion of nano-therapies in clinical stage of the pipeline of pharmaceutical industries [22]. There are many applications of liposomal formulation applied from ophthalmic, cancer chemotherapy and vaccines to gene delivery. A recent review [23], discusses the latest developments in biomedical applications, including highlights of commercially available formulations, clinical trials and patents.

The term "chitosan" refers to a family of pseudo-natural amino polysaccharides obtained at an industrial scale by the chemical deacetylation of chitin, the structural component of the exoskeleton of crustacea, insects and the cell wall of fungi. Chitosan has been widely used in the development of medical devices, given its unique material and bioactive properties, hardly featured by any other single synthetic and natural polymer. Studies showed that liposome stability, payload permeability and cellular delivery could be enhanced by adding a chitosan coating [24–29]. In addition, chitosan and chitosan-coated liposomes have been reported to promote the transport of bioactive macromolecules across epithelial tissues. This has been ascribed to the effect on opening reversibly the tight junctions between epithelial cells [30–32], while interacting with the negatively charged cell membrane, thus enhancing the paracellular permeability of biologics.

There is a gap in studies of liposome or chitosan formulations as buccal delivery vehicles against *P. gingivalis*. Also, the antimicrobial activity of the peptide fragment LL17-32 against *P. gingivalis* is unknown, and how the encapsulation of AMPs in liposome/chitosan formulation affects the antimicrobial activity against *P. gingivalis* is yet to be investigated. In the present study, we studied the influence of three kinds of chitosan of distinct degree of N-acetylation (DA) and molecular weight (Mw), used to coat soybean lecithin (SL) liposomal formulations loaded with peptide LL17-32, on the biophysical and structural properties (size, ζ-potential, morphology, ultrastructure and membrane fluidity). Also, the stability, association efficiency and *in vitro* release of peptide LL17-32 in pristine SL and chitosan-coated SL liposomal formulations were examined. Ultimately, we compared the *in vitro* microbicidal activity against *P. gingivalis* of free peptide LL17-32 and free chitosans, and pristine SL and chitosan-coated peptide LL17-32-loaded SL liposomal

formulations.

2. Materials and methods

2.1. Materials

Biomedical grade chitosans (DA ranging 15–16 %, Mw ranging ~ 39 and 106 kg/mol, see Table S1) were from Heppe Medical Chitosan (HMC+) GmbH (Halle, Germany). The other biomedical grade chitosan sample (DA = 48 %, Mw 164 kg/mol) was from Flexichem (Viscosan) (Uttran, Sweden). Further aspects of the characteristics of the chitosan samples are available in Supporting Information. Soybean lecithin (SL) (powdered soybean lecithin containing a mixture of approximately 46 mol% phosphatidylcholines, 12–17.4 mol% phosphatidylinositol, 3–7 mol% phosphatidylglycerol, 0–1.5 mol% phosphatidic acid, phosphatidylethanolamine, and trace amounts of triglycerides, cholesterol, and fatty acids [33]) was purchased from VWR Chemicals (CAS: 8030-76-0, Leuven, Belgium). Peptide LL17-32 (FKRIVQRIKDFLRNLV) was purchased from CPC Scientific Inc. (San Jose, CA). Cholesterol (≥98 %) (CAS: 57-88-5), N-acetyl-glucosamine and Blood Agar were purchased from Sigma Aldrich (St. Louis, MO). *P. gingivalis* W83 strain was purchased from the American Type Culture Collection (ATCC, Manassas, VA, USA). Brain heart infusion broth was purchased from EO Labs (Bonnybridge, UK). Horse Blood was purchased from Thermo Fisher Scientific (UK). Laurdan (CAS: 74515-25-6) was purchased from Cayman Chemicals (MI, USA). The other chemicals were of analytical reagent grade or higher.

2.2. Preparation of chitosan-coated/uncoated liposomes

In this study, the thin-film hydration method [34] was used to prepare peptide LL17-32 loaded and unloaded liposomes. Briefly, for a typical batch preparation, SL and cholesterol were dissolved in chloroform at a concentration of 12 and 2 mg/mL (i.e., ~27 mol% cholesterol), respectively. The organic solvents were evaporated by bubbling a dry nitrogen stream in a fume hood, followed by placing the flask on a vacuum pump overnight to remove the residual organic solvent. The large multilamellar vesicles (LMVs) were formed by re-suspending the dry lipid film in 10 mM NaCl (pH = 4.5) and the final concentrations of lipids and cholesterol were identical to the original ones in the chloroform solution (12 and 2 mg/mL, respectively). The LMV suspension was then placed in a water shaking bath (Elmasonic S 10H, Elma, Singen, Germany) at 46 °C at 200 rpm for 15 min, and subsequently disrupted by extrusion through a 100 nm polycarbonate membrane with a block holding mini-extruder (61000, Avanti Polar Lipids, USA) at 60 °C to yield large unilamellar vesicles (LUVs) with a diameter of ~120 nm. The same protocol was used to prepare the peptide LL17-32-loaded liposomes, but in this case, a constant amount of the peptide (600 μg/mL) was added to the water phase (pH = 4.5, 10 mM NaCl) before the hydration step (1.1 mol%). Fluorescently labelled liposomes were prepared by adding the mixture of Laurdan, lecithin and cholesterol in chloroform, to a final lipid concentration of 0.1 g/L and Laurdan concentration of 2 μM.

To prepare chitosan-coated liposomes, chitosans of varying degrees of acetylation (DA) and Mw were dissolved in 10 mM NaCl and 5 % stoichiometric excess of HCl (as per equivalent D-glucosamine) under continuous magnetic stirring overnight, followed by adding liposome dropwise to the same amount of chitosan at a concentration of 2, 3 and 4 mg/mL. The final nanoparticles: unloaded/loaded SL liposome (Unloaded/loaded-SL), Chitosan 80/20® coated SL liposomal LL17-32 (HMW-LDA-unloaded/loaded-SL), Viscosan® coated liposomal LL17-32 (HMW-HDA-unloaded/loaded-SL), Chitosan 85/5® coated SL liposomal LL17-32 (LMW-LDA-unloaded/loaded-SL) were stored at 4 °C in the dark and used for characterization.

2.3. Particle size and ζ-potential analysis

Measurements of particle size distribution and polydispersity (PDI) were determined by determining the apparent values of the hydrodynamic radius R_h, (related to the diffusional dynamics of a vesicle) by non-dynamic light scattering with non-invasive back scattering (DLS-NIBS) at 173°. The R_h determination was made by means of the Stokes–Einstein relation using the diffusion coefficient D_{APP} determined by Eq. (1)

$$D_{APP} = \frac{K_B T}{6\pi\eta_0 R_h} \tag{1}$$

Where K_B is the Boltzmann constant, T is the absolute temperature, η_0 is the viscosity of the solvent and R_h is the hydrodynamic radius.

For each liposome preparation, DLS-NIBS measurements were performed immediately after the samples were prepared and after 33 days stored at 4 °C. Liposome suspensions were diluted 100-fold with water in plastic disposable cuvettes and equilibrated at 25 °C before measurements were recorded. Each measurement was taken four times. The ζ-potential, indicative of particle surface charge, was determined by mixed laser Doppler velocimetry and phase analysis light scattering (M3–PALS) from the values of electrophoretic mobility (μe) using Henry's equation Eq. (2)

$$\mu e = \frac{(2\varepsilon\zeta f(Ka))}{3\eta} \tag{2}$$

Where f(Ka) is the Smoluchowski's approximation (1.5), ε is the dielectric constant of the dispersant (water), η is the viscosity of solvent.

Both types of measurements were conducted using a Malvern Zetasizer ZEN5600 (Malvern Instruments, Worcestershire, UK)

equipped with a 4 mW He/Ne laser beam (λ = 633 nm).

2.4. In vitro RTF release study

A dialysis tube (MWCO 10 KDa) containing 0.3 mL of liposome formulation was incubated in 30 mL reduced transport fluid (RTF) (2.5 mM dipotassium hydrogen phosphate, 3 mM potassium dihydrogen phosphate, 20 mM NaCl, 1.2 mM ammonium sulfate, 4 mM sodium carbonate, 1.5 mM dithiothreitol, and 10 % EDTA) (pH 7.1) at 37 °C with continuous shaking at 80 rpm (GRANT-JBA5, Germany). An aliquot of the mixture was withdrawn at appropriate time intervals (0.5, 1, 2, 4, 8, and 24 h). Before determining the concentration of released LL17-32 in the mixture, Genevac (7EZ-2 plus, UK) at the mode of aqueous condition at 30 °C was used to evaporate excess water and concentrate the released peptide. Released LL17-32 was detected, using the reversed-phase HPLC method as described above. Free LL17-32 was tested as a control and the released rate was quantified by Eq. (4):

$$\text{Release rate } (\%) = \frac{\text{Released}_{\text{LL17-32}}}{\text{Total}_{\text{LL17-32}}} \cdot 100 \tag{4}$$

2.5. Physical stability in RTF

The colloidal stability of nanoparticles in RTF (pH 7.1) was studied from the evolution of the particle size distribution from DLS-NIBS measurements at varying time intervals up to 4 h at 37 °C using the DLS-NIBS described in **Section 2.3**.

2.6. Liposome membrane fluidity

To determine the effect of LL17-32 peptide and chitosan on the SL membrane fluidity, Laurdan (2-dimethylamino-6-lauroylnaphthalene) was used as a membrane fluorescent probe [35]. Laurdan, is a solvent-sensitive compound with a donor and an acceptor part localised opposite to the naphthalene ring. It is known to insert in the phospholipid bilayers via its 12-carbon aliphatic chain leaving the fluorescent naphthalene ring close to the membrane surface, leading to a large electric dipole. In lipid membranes, Laurdan emits at around λ = 440 nm in a gel bilayer, but at λ = 490 nm in a liquid crystalline membrane. A generalised polarisation (GP) can be calculated from the normalised intensity relationship of both intensities given by Eq. (5):

$$GP = (I_{440} - I_{490}) / (I_{440} + I_{490}) \tag{5}$$

where I_{440} and I_{490} are the fluorescence emission intensity at λ_{em} = 440 nm (gel phase) and the fluorescence emission intensity at λ_{em} = 490 nm (liquid crystalline phase), respectively. Laurdan-labelled liposomes were prepared as described in **Section 2.4**. Briefly, diluted fluorescent samples were placed in quartz cuvettes. The fluorescence emission spectra were obtained with an excitation wavelength λ_{ex} = 340 nm by an FP-8500 spectrofluorometer (JASCO applied science, Halifax, Canada), using 2.5 nm slits. Spectra were recorded from λ = 400 nm–600 nm at 37 and 75 °C. It is important to note that Laurdan has also been widely employed in previous studies to assess the lipid packing degree in the liquid crystalline phase (Lα-phase), providing a theoretical range of values from +1 (indicating the highest level of order) to −1 (representing the lowest level of order) [36].

2.7. Small-angle X-ray scattering (SAXS)

SAXS measurements were conducted at Diamond-Leeds SAXS Facility (Diamond Light Source, Didcot, U.K.) using a Xeuss 3.0 instrument (Xenocs, Grenoble, France) equipped with a Liquid Gallium MetalJet (Excillum, Krista, Sweden) under the approved beamtime experiment ref. no. SM30751. The following settings were used: X-ray generator voltage of 70 kV with a wavelength λ = 0.134 nm, a sample-to-detector distance: 4510.76 mm, providing a q range of 0.14–8 nm^{-1}. The exposure time was 600 s. An Eiger2 1 M detector (Dectris AG, Baden-Daettwil, Switzerland) was used to collect the data. No beam-stop was used. The dispersions with a concentration of 1.8 wt% were loaded into polycarbonate capillaries (2 mm outer diameter and 1.6 mm inner diameter), and vacuum sealed with a plastic plug and a fast-setting epoxy. A Peltier temperature-controlled capillary holder was used to obtain temperature stability (± 0.1 °C once temperature stable). The measurements were conducted at 25 and 75 °C. Data were processed according to the standard processing pipeline in DAWN. This included q calibration based using silver behenate powder with a d-spacing of d = 5.838 nm, masking of unwanted pixels, correction for the sample transmission, subtraction of the background and the azimuthal integration. For background subtraction, the intensities from the empty capillary and then from the solvent medium (10 mM NaCl) were subtracted.

The scattered intensities versus q (nm^{-1}) were further analysed using the global analysis method, enabling the simulation of full q-range scattering profiles and obtaining a quantitative understanding of the structural and fluctuation behaviour of the systems. Detailed information about the models applied to simulate both form and structure factors in multilamellar vesicles has been described in the literature [37–40]. Briefly, we have used a 2-Gaussian model for the electron density profile of the lipid bilayer, where its Fourier transform is calculated to represent the bilayer scattering form factor. The modified Caillé theory (MCT) has been used to simulate the structure factor [41,42]. We note that the prepared samples were a mixture of unilamellar and multilammelar vesicles. Hence, the total scattering intensity was described by a linear combination of the scattering from every one of those systems, *i.e.*, $I(q) = \propto \left[F(q)^2\right] / q^2 + (1 - \propto) \left[S(q).F(q)^2\right] / q^2$, where $F(q)$ is the form factor, $S(q)$ is the structure factor and ∝ is the weighing factor indicating the

unilamellar vesicles fraction in the hybrid mixture. The applied structure factor model enables obtaining a quantitative fluctuation parameter called Caillé parameter, η [43]. The weighing factor, the Caillé parameter, the repeat distance of multilamellar vesicles and the average bilayer thickness of monolayers, along with other parameters describing the total scattering intensities, were obtained by fitting the experimental scattering data. We applied an advanced particle swarm optimisation (PSO) algorithm in a MATLAB environment to find the best solution for this multiple-fitting problem and avoid entrapment into local minima [38,40].

2.8. Bacteria-killing activity against Porphyromonas gingivalis

P. gingivalis W83 strain was cultured using a method adapted from Curtis *et al.* [44]. Briefly, bacteria were grown in brain heart infusion (BHI) broth and incubated in an anaerobic chamber (10 % H_2, 10 % CO_2, 80 % N_2) (Whitley M55 Workstation, UK) reaching the late logarithmic phase. Then, washed twice and resuspended in reduced transport fluid (RTF) (pH 7.1) to an optical density at $\lambda =$ 600 nm corresponding to 10^6 colony-forming units per millilitre (CFUs/mL). Peptide LL17-32 was serially diluted in RTF and an equal volume of 100 μL bacterial suspension was added, to give final peptide concentrations ranging from 3.75 μg/mL to 30 μg/mL. After 30 min incubation, 20 μL aliquots were subject to a 1:10 serial dilution in RTF and, viable counts were quantified by inoculation onto blood agar plates. For free chitosan solutions and pristine SL and chitosan-coated SL peptide LL17-32-loaded liposomal formulations, two incubation periods (30 min or 4 h, respectively) were used and the final concentration of chitosan and LL17-32 in liposome samples was set as 0.2 mg/mL and 30 μg/mL, respectively. The viability rate was calculated by **Eq. (6)**:

$$\text{Viability rate}(\%) = \frac{\text{CFUs of the test sample}}{\text{CFUs of the control (untreated)}} \cdot 100 \tag{6}$$

2.9. Statistical analysis

All experiments were carried out in triplicates (except SAXS). Results were expressed as means ± standard deviation. Comparisons were made by paired Student's *t*-test analysis using GraphPad Prism version 9.4.1 for Windows, GraphPad Software (San Diego, California USA, www.graphpad.com). Differences were significant at $p < 0.05$ throughout this study.

3. Results and discussion

3.1. Characterisation of chitosan samples

Previous studies have consistently documented the effect of chitosan to stabilise liposomes and improve their mucoadhesive properties [24–27]. Chitosan is a promising polysaccharide in this regard because it can coat the surface of liposomes by electrostatic interaction, thereby increasing stability. In this work, three chitosans of biomedical purity varying in their major structural properties, namely the molecular weight (Mw) and the degree of N-acetylation (DA), were used and their characterisation methods and data are shown in Table S1. Samples HMW-LDA and HMW-HDA both had a high Mw (106 and 164 kDa, respectively) and widely distinct DA (16 and 48 %, respectively). Meanwhile, samples HMW-LDA and LMW-LDA both shared similar DA (~15–16 %) and distinct Mw (106 and 39 kDa, respectively) (Table S1, Fig. S1).

Of note, the polydispersity (Đ) of the three samples was very close (Đ ~1.6–1.7). To have carried out a more extensive study using

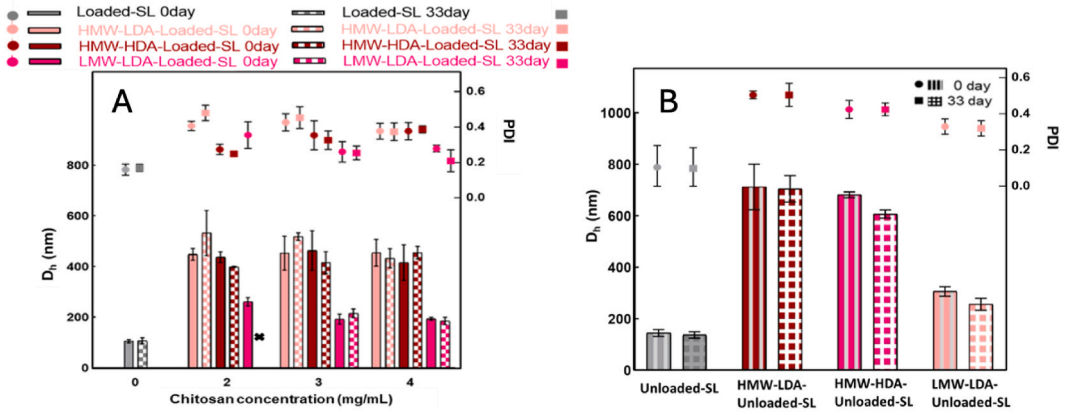

Fig. 1. Variation of the average hydrodynamic diameter (D_h) and polydispersity (PDI) of: (A) LL17-32 peptide loaded (0.6 mg/mL) soy lecithin (SL) liposomes coated with chitosans (HMW-LDA, HMW-HDA and LMW-LDA) at varying concentrations or pristine; and (B) Unloaded soy lecithin (SL) liposomes coated with chitosans (HMW-LDA, HMW-HDA and LMW-LDA) at 4 mg/mL or prisitine. All formulations were evaluated at 0 and after 33 days of storage at 4 °C (as per legend) (pH = 4.5, 10 mM NaCl, 25 °C, total lipids concentration 7 mg/mL, average ± SD, n = 3). Symbol "X" in panel A denotes an unstable precipitated sample.

chitosans of varying Mw and DA over a broader range of values than those used in the present work lay beyond the scope of this study. Notwithstanding, the selected chitosans enabled us to conduct insightful comparisons of the influence of these two parameters on the structure of the phospholipidic membrane, stability and biological properties of the liposomal formulations. As previously noted, numerous early published reports and more recent ones utilized poorly characterized samples that lack data on chitosan's Mw or DA. Furthermore, in contrast to the chitosans utilized in this study, with varying DA, the majority of previous studies have exclusively employed low DA (<~25 %) chitosan to coat the surface of liposomes [28,45–47]. Of note, chitosan's DA plays a critical role in modulating the interactions between the polymer and the liposome's surface, as further discussed in subsequent sections.

3.2. Characterization of particle size and polydispersity

To investigate the unloaded and LL17-32 peptide-loaded pristine SL liposomes (unloaded/loaded-SL) and the influence of the addition of varying concentrations of chitosan (2.0, 3.0 and 4.0 mg/mL) on the physical properties, DLS-NIBS and ζ-potential measurements were performed immediately after preparation and after 33 days of storage in refrigeration (4 °C). The loading of uncoated SL liposomes with the peptide LL17-32 was associated with a reduction in their average particle size of ~20 nm. The PDI in all the pristine formulations remained invariably ~0.2, indicative of a narrow size monomodal particle size distribution Fig. 1A and **B**.

A few studies have already investigated the influence of peptide LL-37 on the characteristics of lipid membranes in liposomes [18,48–50]. Previous works by Ron-Doitch *et al.* [50] documented the encapsulation of peptide LL-37 in PEGylated liposomes and found an average hydrodynamic diameter of ~100 nm, in good agreement with the size of peptide LL17-32-loaded SL liposome (Loaded-SL) determined in our study. However, they did not report the data for unloaded pristine liposomes. Also, to the best of our knowledge, there have been no previous reports on the LL17-32 fragment responsible for the antimicrobial activity of LL-37 peptide. In general, particle size depends not only on the characteristics of the given payload and different preparation methods but also on lipid composition and cholesterol level [51]. We reason that the ~20 nm reduction in SL liposome diameter resulting from LL-17-32 loading, occurs due to the peptide inducing a re-arrangement of the original structure of the lipid membrane. In this regard, we can speculate that there is a change from a non-interdigitated structure to a quasi-interdigitated phase (Fig. S4). In overall agreement with this proposal, a previous study [49] using SAXS, has shown that 4 mol% LL-37 alters the diffuse scattering of pure DPPG. This suggests that there is a decrease in the positional correlations between the bilayers. Further analysis of the scattering data revealed that the phosphate-phosphate distance ($d_{PP=}2^{\cdot}zH$) of the liposome membrane is around 3.1 nm, a significantly smaller value compared to when the peptide is absent (zH = ~2.2 nm). The formation of quasi-interdigitated structures can be explained as the consequence of the amphipathic character of LL-37. When it interacts with a lipid bilayer, the most likely organization is for the peptide to align parallel to the plane of the bilayer. This positioning shields the hydrophobic tail ends of the lipids from the surrounding aqueous solution, thus resulting in a quasi-interdigitated structure. As the peptide monomers align themselves parallel to the bilayer plane, the headgroups of the lipids in the bilayer tilt away from their orientation parallel to the membrane surface. This configuration allows for tighter packing of the hydrocarbon chains in this phase. Furthermore, the presence of LL-37 can also lead to the formation of disk-like micelles with a diameter of ~27 nm and a bilayer thickness of ~5 nm (Fig. S4). Many other factors are likely to influence peptide/lipid assemblies. These can include peptide-to-lipid ratio, types of lipids and peptides, hydration levels of the bilayer, and electrostatic factors [52–56]. While the formation of interdigitated assemblies during the preparation or extrusion step may contribute to the smaller size of peptide-loaded liposome systems compared to unloaded ones, the primary reason for the different sizes in our study is likely to be due to differences in membrane fluidity. Specifically, peptide LL17-32 unloaded liposomes have been shown to exhibit higher membrane fluidity than the loaded ones, as will be further discussed in **Section 3.5**. Liposomes with a high membrane fluidity can compress and pass through membrane pores without being disrupted, thereby maintaining their original size. In contrast, we can speculate that liposomes with more rigid membranes are more likely to be torn apart and re-assemble into smaller vesicles. The influence of the chitosan type (HMW-LDA, HMW-HDA, and LMW-LDA) and chitosan concentration (2–4 mg/mL) on the D_h and PDI of peptide LL17-32 loaded liposomes (loaded-SL) are shown in Fig. 1A panel. The corresponding values (D_h, PDI) for unloaded SL liposomes coated with 4 mg/mL of the three chitosans are shown In Fig. 1B panel. Experimental trials were conducted to establish the best prototype chitosan-coated liposomal formulations. To this end, HMW-LDA chitosan was added to pristine SL liposomes at varying chitosan/lipids mass ratios in the range of 0–1.0 and determined the variation of D_h and ζ-potential (Fig. S5). It was observed that as the chitosan contents increased an increase followed by a sharp decrease in D_h accompanied the inversion of the ζ-potential from highly negative (~-44 mV) to highly positive (~+42 mV). Little variation on both parameters was achieved at mass ratios of ~0.1 and beyond evidencing the saturation of the liposome surface, in agreement with previous independent studies [45,57]. Therefore, formulations in the range of mass ratios of 0.3–0.6 (chitosan conc. 2–4 mg/mL) were selected for peptide LL17-32 loading and further studies.

Notice in Fig. 1A, that after coating, loaded-SL with chitosans at the selected concentrations (2–4 mg/mL), the average D_h of the formulations showed a ~2–~4-fold increase as compared with the pristine loaded-SL one. A closer inspection of the figure reveals that the D_h of high molecular weight chitosans (HMW-HDA and HMW-LDA) at concentrations of 3 and 4 mg/mL the D_h is twice as large as those coated with the low molecular weight chitosan (LMW-LDA). This is rationalised as the result of the formation of long polyelectrolyte chains on the high Mw chitosans that would tend to form Gaussian coils and loops instead of flat chains ("trains") adsorbed at the liposome's surface [47]. By contrast, shorter polyelectrolyte chains in the low Mw chitosan (LMW-LDA) would be expected to pack more densely on the phospholipidic surface than the longer high Mw counterparts due to an entropic advantage associated with their greater overall mobility and number, in agreement with previous results in chitosan-coated nanocapsules [58]. Across all three chosen chitosan concentrations within the same type of chitosan, within experimental error, few differences were observed on both size and PDI. However, liposomes coated with LMW-LDA at the lowest concentration (2 mg/mL), showed ~30 % greater size and PDI than at higher concentrations (3 and 4 mg/mL). Also, this sample showed aggregation after 33 days of refrigerated storage and could

not be measured. Based on the observed instability of this system, it is possible that a higher concentration of low Mw chitosan (LMW-LDA) is required to achieve saturation on the liposome's surface and ensure the system's stability over long-term storage. This lower saturation and dense packing of the liposome's surface proposed for the low Mw chitosan may also explain the reduction in size as the chitosan concentration increased from 2 to 3 mg/mL ζ-Potential data are in agreement with this interpretation as discussed further in **Section 3.3**. The greater charge density of low DA chitosan is expected to favour stronger electrostatic attractions with the liposome's surface than high DA chitosan [45,59]. This could have a consequence on the overall adsorption and thickness of the chitosan coat around the liposomal surface. However, within experimental error, no differences in particle size were noticed between HMW-HDA and HMW-LDA chitosan-coated formulations. We reason that either the differences in coat thickness are proportionally too small or high DA chitosan does interact to the same extent as low DA by other mechanisms such as hydrophobic forces.

The particle size of LL17-32 unloaded chitosan-coated liposomes (chitosan conc. 4 mg/mL) was found to be larger by ~25–30 % than that of the peptide-loaded formulations (*cf*. Fig. 1B vs. Fig. 1A). These results agree well with those shown for unloaded pristine SL liposomes that were larger than the loaded equivalent, as previously discussed. Of note, no size reduction steps were applied after the chitosan-coating process. In addition, the particle size and PDI values showed a similar trend for the peptide-loaded formulations, where the high Mw chitosan-coated liposomes had a larger average size and higher PDI compared to the low Mw chitosan-coated alternative.

3.3. ζ-potential

The ζ-potential data corresponding to the pristine and chitosan coated SL liposomal formulations are shown in Fig. 2. A first observation to note is that unloaded systems' ζ-potential had a greater ζ-potential slightly from ~ −45 to ~ −38 mV for SL liposome after loading with LL17-32. This is not unexpected purely on electrostatic grounds given the high isoelectric point of LL17-32 peptide (pI = 12) that results in a net positive charge at the working pH that partially neutralises and binds to the lipid head groups of phospholipids. This result is consistent with the notion that LL17-32 attaches not only at the inner lipid surface in contact with the aqueous core but also at the outer surface of the lipid bilayer. SAXS studies may shed further light to elucidate in greater detail whether helical LL17-32 molecules locate parallel on the bilayer surface or induce the formation of quasi-interdigitated structures (Fig. S4). In good agreement with the size data, both types of formulations showed to remain stable during refrigerated storage for at least 33 days.

As expected, after coating SL liposomes with the three types of chitosan, the ζ-potential inverted from negative to ~+40 mV (Fig. 2). This result indicated that the chitosan coated the surface of the liposome by electrostatic interaction between the positively charged amine group of chitosan and the negatively charged phosphate group of liposomes. As expected, the low degree of acetylation (HMW-LDA and LMW-LDA) chitosan formulations loaded showed consistently greater ζ-potential values than the HMW-HDA systems comprising chitosan with an overall lower proportion of protonated D-glucosamine amino groups. Also, note in Fig. 2A that higher concentrations of chitosan showed slightly increased charge ζ-potential values. It is interesting that by comparing different molecular weights of chitosan coating at a similar degree of acetylation (DA) and identical concentration, low Mw chitosan-coated liposomes showed a slightly lower ζ-potential than high Mw chitosan-coated ones. This can be reasoned as the consequence of the greater amount of low Mw chitosan needed to saturate the anionic liposomal surface with respect to the high Mw chitosan with an overall greater degree of space occupancy at an equivalent concentration. Similar results have also been reported by Bang *et al.* [46] who determined that the ζ-potential of chitosan increases with its molecular weight.

For peptide-unloaded liposomes coated with 4 mg/mL of either of the three chitosans (Fig. 2 B), the variation in ζ-potential values seem consistent with the values for the peptide-loaded liposomes, where low degree of acetylation (LDA) chitosan-coated systems presented higher ζ-potential values than the high DA formulations. Also, high Mw chitosan-coated liposomes showed a slightly higher

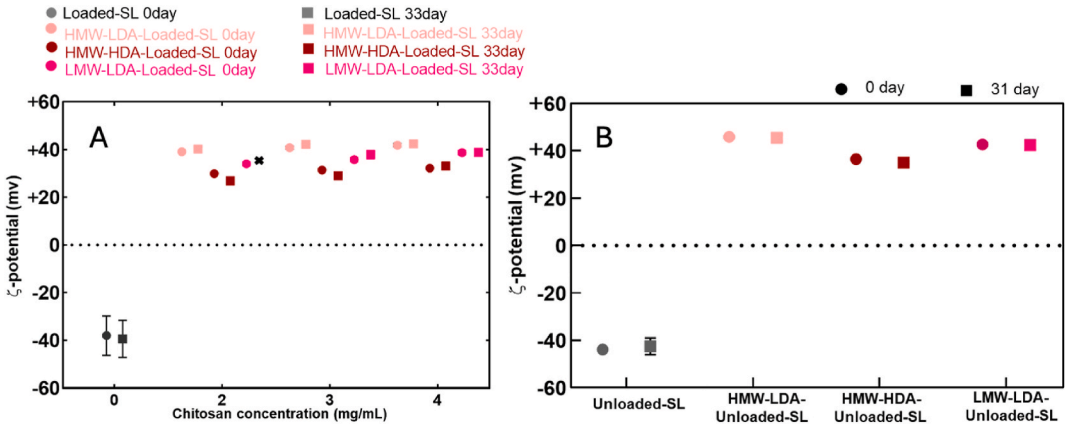

Fig. 2. Variation of the ζ-potential of chitosans (HMW-LDA, HMW-HDA and LMW-LDA) at varying concentrations coated or pristine LL17-32 loaded (0.6 mg/mL) SL liposomes (Loaded-SL) (A); chitosans (HMW-LDA, HMW-HDA and LMW-LDA) at 4 mg/mL coated LL17-32 unloaded SL liposomes and pristine LL17-32 unloaded (0.6 mg/mL) SL liposomes (unloaded-SL) (B). All formulations were evaluated at 0 and after 33 days of storage at 4 °C (as per legend) (pH = 4.5, 10 mM NaCl, 25 °C, average ± SD, n = 3). Symbol X in panel A denotes an unstable precipitated sample.

ζ-potential than low Mw chitosan-coated ones. Liposomes coated with HMW-LDA presented overall greater stability during refrigeration storage for 33 days. This may be attributed to the colloidal stabilisation brought by the prevalence of repulsive electrostatic interactions in all the chitosan-coated liposomes, with invariably high ζ-potential. Many researchers have suggested that coating liposomes with chitosan, improves stability [57,60,61]. However, in our study, the pristine liposomal LL17-32-loaded formulation was also stable during prolonged refrigeration storage.

3.4. Transmission electron microscopy (TEM) imaging studies

TEM imaging provided further insight of the size and surface morphology of the unloaded and peptide-loaded liposomes of different kind. Invariably, the liposomes exhibited a mostly spherical morphology with subtle structural variations in their structure (Fig. S6). The use of uranyl acetate as contrast agent, expected to bind to phosphate groups of phospholipids [62], resulted in positive stained images. However, obtaining clear-edge vesicle images of uncoated SL liposomes was challenging. We reason that the difficulty stemmed from the repulsive interaction between the high negative charge on the SL liposomes surface and the negatively charged carbon-coated film of the grid. This repulsive force may have prevented the liposome samples from adsorbing efficiently onto the grid surface, thus making it difficult to obtain clearer images.

Upon coating SL liposomes with the three types of chitosan, the particle size of the observed small vesicles seemed not to increase with respect to the uncoated systems. This observation did not concur with results from DLS-NIBS that showed up to four-fold greater diameter for the coated liposomes than the pristine ones. In DLS-NIBS, larger particles scatter more light than smaller particles do, and hence, the intensity of the scattered light is more strongly influenced by the presence of larger particles. Therefore, the intensity-based DLS-NIBS size measurements are biased towards the contribution of the larger particles to the scattering while that of the smaller particles is less prominent. As noticed in the TEM images, a large amount of small-sized (~30 nm) particles are present in the chitosan-coated formulations. Also, it is important to note that the intensity-based size measurement in DLS-NIBS provides information about the bulk hydrodynamic radius of a hypothetical sphere that would diffuse at the same rate as the particles in the solution. Moreover, the differences in size and polydispersity observed between TEM and DLS-NIBS could be attributed to the condition of preparation of the specimens for TEM imaging such as the adsorption in the grids, staining with uranyl acetate, use of high vacuum while recording images.

Even after considering these aspects, no major morphological differences were observed among the three different chitosans-coated liposome samples. Especially, HMW-HDA-loaded-SL TEM images (Fig. S6) showed smaller particles than those comprised by the DLS-NIBS particle size distribution (not shown). Also, this result is discrepant with data from DLS-NIBS that showed that low Mw chitosan-coated liposomes were smaller than high Mw chitosan-coated ones (*cf.* Fig. S6, respectively). We venture to suggest that the adsorbed chitosan layer dissociated from the liposome surface during the specimen grid preparation. This could be due to the interference between negatively charged carbon film on the grids and the positively charged amine group of chitosan or/and the formation of aggregates after adding uranyl acetate solution. In agreement with this suggestion, the presence of dark-coloured larger spherical

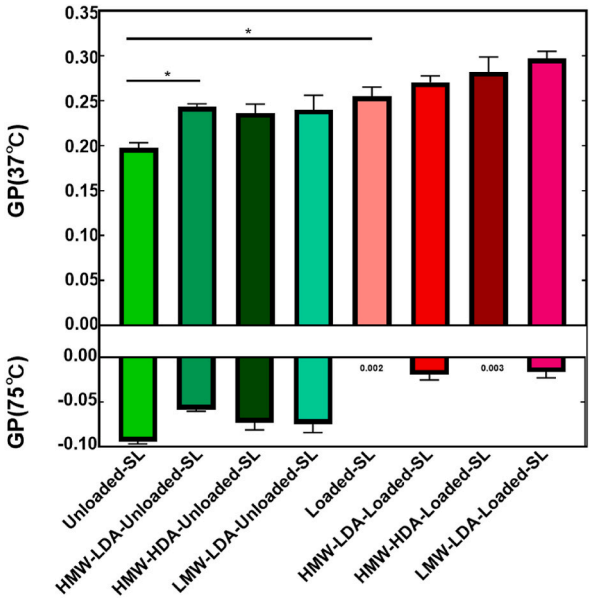

Fig. 3. Variation of the generalised polarisation (GP) of SL lipid membrane in unloaded and LL17-32 peptide-loaded (0.6 mg/mL) chitosan (4 mg/mL) coated and pristine loaded liposomal formulations. GP values calculated for each sample are presented as means ± SD ($n = 3$) at 37 and 75 °C; Pairwise Student's t-test statistical comparisons between the Unloaded-SL and HMW-HAD-unloaded-SL, and between Unloaded-SL and Loaded-SL (*$p < 0.05$).

particles in some images (Fig. S6 and **H**), could be due to chitosan-coated liposomes that remained undissociated, since their size was relatively close to the D_h data from DLS-NIBS. Of note, multilamellar vesicles were also observed in chitosan-coated samples as shown for a representative image of in HMW-HDA chitosan-coated LL17-32 loaded-SL liposome (Fig. S7). In this case, chitosan seems not to be coating the surface of liposomes and multilamellar vesicles. These structures are most likely formed during liposome preparation, and even after extrusion through 100-nm diameter pores, they remain, as shown in previous studies [63]. There are several challenges associated with imaging chitosan nanoparticles by TEM including the sensitive nature of the material, low contrast, instrument limitations, and sample thickness. Specifically, chitosan particles can be prone to aggregation, making it difficult to obtain a uniform specimen for imaging [64]. To overcome these challenges, careful sample preparation and imaging conditions, as well as advanced imaging techniques such as cryo-TEM, may be necessary in future studies.

3.5. Liposome membrane fluidity and structure

The sustained membrane fluidity is crucial for normal cellular metabolism [65]. Membrane fluidity is the degree of molecular disorder and molecular motion within a lipid layer [66]; therefore, it was an important parameter to investigate for the developed liposomal systems using Laurdan fluorescence spectroscopy at 37 and 75 °C. As shown in Fig. 3, at 37 °C, LL17-32 unloaded and loaded pristine SL liposomes have generalised polarity (GP) values of approximately 0.2 and 0.25, respectively. These positive GP values can correspond to the liquid-ordered phase (L_o-phase) of the membrane [36]. Soybean lecithin (SL) is a complex mixture of various phospholipids, with phosphatidylcholine (PC) (~45 mol%), phosphatidylethanolamine (PE) (~20 mol %), and phosphatidylinositol (PI) (~15 mol%) being the most abundant components [33]. These phospholipids encompass a combination of saturated, monounsaturated, and polyunsaturated fatty acids. Notably, linoleic acid (C18:2), oleic acid (C18:1), and linolenic acid (C18:3) are among the most prevalent fatty acids present. Although SL also contains significant amounts of saturated phospholipids present, such as palmitic acid (C16:0) and stearic acid (C18:0) [33], it is noteworthy that approximately 80 % of these in soybean lecithin are unsaturated. This composition significantly influences the phase equilibrium and transition temperature (T_m) of the membrane.

Consequently, the overall T_m of SL remains below 0 °C due to the predominance of unsaturated phospholipids. For example, the T_m of soybean PC and PE have been reported to lie between approximately −25 and −11 °C, respectively [67]. Importantly, in our SL liposome system, we supplemented approximately 27 mol% of cholesterol, which could induce the transition of saturated phospholipids from the liquid-disordered phase (LD-phase) to the liquid-ordered (L_o) phase. We propose that the SL liposome system exists in a liquid phase with free lateral movement of lipids, but it does not exhibit the characteristics of either the L_d or fully L_o phase. However, the presence of saturated phospholipids and the measured high positive GP values in SL-loaded and SL-unloaded liposomes at 37 °C, suggest the coexistence of the L_d and L_o phases in the SL liposome system.

As the temperature increased to 75 °C for the SL liposomes, the GP values decreased to ~0 and ~-0.1 for loaded and unloaded liposomes, respectively. This indicates that most phospholipids in SL changed to their liquid-disordered (L_d) phase. Although the presence of the 27 mol% of cholesterol can result in a liquid-ordered (L_o) phase for phospholipids with high saturation degree [68], and L_o-L_d coexistence at a temperature higher than their T_m, at 75 °C and the low GP values, are diagnostic that a temperature above the critical point has been reached, where the L_o and L_d phases no longer coexist and a the membrane is in a fluid state. A temperature-dependent phase diagram for DOPC/DPPC/cholesterol was proposed by Veatch *et al.* [69]. In this study, it was shown the coexistence of a L_o-L_d region that expands at lower temperatures and shrinks at higher temperatures, and these L_d and L_o phases can no longer coexist at a temperature higher than ~30 °C. Again, the lack of a defined phospholipid profile in SL makes determining the liposome's specific phase state challenging. Hence, we reason that our observations are consistent with the notion that an increase in temperature results in increased membrane fluidity due to the vanishing of the L_o phase at 75 °C.

Interestingly, loading of LL17-32 peptide significantly ($p < 0.05$) decreased the membrane fluidity of SL systems at both temperatures. To the best of our knowledge, no such finding related to the influence of peptide LL17-32 in inducing membrane fluidity change has been published. However, Sevcsik *et al.* [49] reported that peptide LL-37 induced tighter and increased ordered hydrocarbon chain packing using SAXS and WAXS. The interdigitated structure suggested in Section 3.2 (Fig. S4) and the strong affinity between oppositely charged peptide and SL could be the reason for the decreased fluidity of the SL membrane after loading peptide LL17-32. In agreement with this, a study investigated the effect of cationic alpha-helix peptide ascaphin-8 and its variants on membrane fluidity by using Laurdan fluorescence spectroscopy [70]. The results showed that in the POPC:POPG (80:20) membrane model, each peptide contributed to the membrane rigidity. However, none of the peptides caused any observable fluidity iterations in the POPC:ERG (ergosterol) (70:30) or POPC:CHL (cholesterol) (70:30) systems. Again, the interactions of peptides and lipid membranes can be affected by a variety of factors, including the properties of the peptide (*e.g.,* pI, hydrophobicity, sequence, size), the lipid composition, the concentration of the peptide and lipids, and the presence of other molecules or ions, pH, temperature. The possibility that the short LL-17-32 peptide fragment could adopt an amphipathic helical conformation to explain some of the observations on membrane fluidity cannot be ruled out either.

The influence of chitosan coatings on the fluidity of SL liposomes was also investigated. Of note, all three kinds of chitosans included in this study decreased ($p < 0.05$) the fluidity of the membrane for both peptide-loaded and unloaded SL liposomes, as noticed by the increase in GP values (Fig. 3). Embedding of the chitosan's hydrophobic GlcNac (A) residues in the SL liposome membrane driven by hydrophobic interactions with the alkyl chain of the phospholipid could explain the decreased membrane fluidity. Tan *et al.* [71], examined the membrane fluidity using three fluorescence probes inserted on the outer membrane surface, superficial region, and hydrophobic core. They found that when the chitosan concentration was greater than 1 mg/mL, the coating significantly decreased the membrane fluidity, and this modifying ability was the strongest on the membrane surface. It was expected that HMW-HDA and LMW-LDA chitosan would have the most significant impact on membrane fluidity. This is because high DA chitosan has more exposed

hydrophobic acetyl groups (from A residues), while low Mw chitosan presents shorter polyelectrolyte chains, which tend to have a denser packing on the lipid membrane, hence the greatest decrease in the lipid membrane fluidity. A previous study [28], showed that the fluidity of liposomes coated with high Mw chitosan is significantly less than that of liposomes coated with low Mw chitosan. This indicates that the extended molecular chains of high Mw chitosan result in a greater restriction of the longitudinal motion of phospholipid molecules. However, in our study, no significant differences were observed in the membrane fluidity among the three

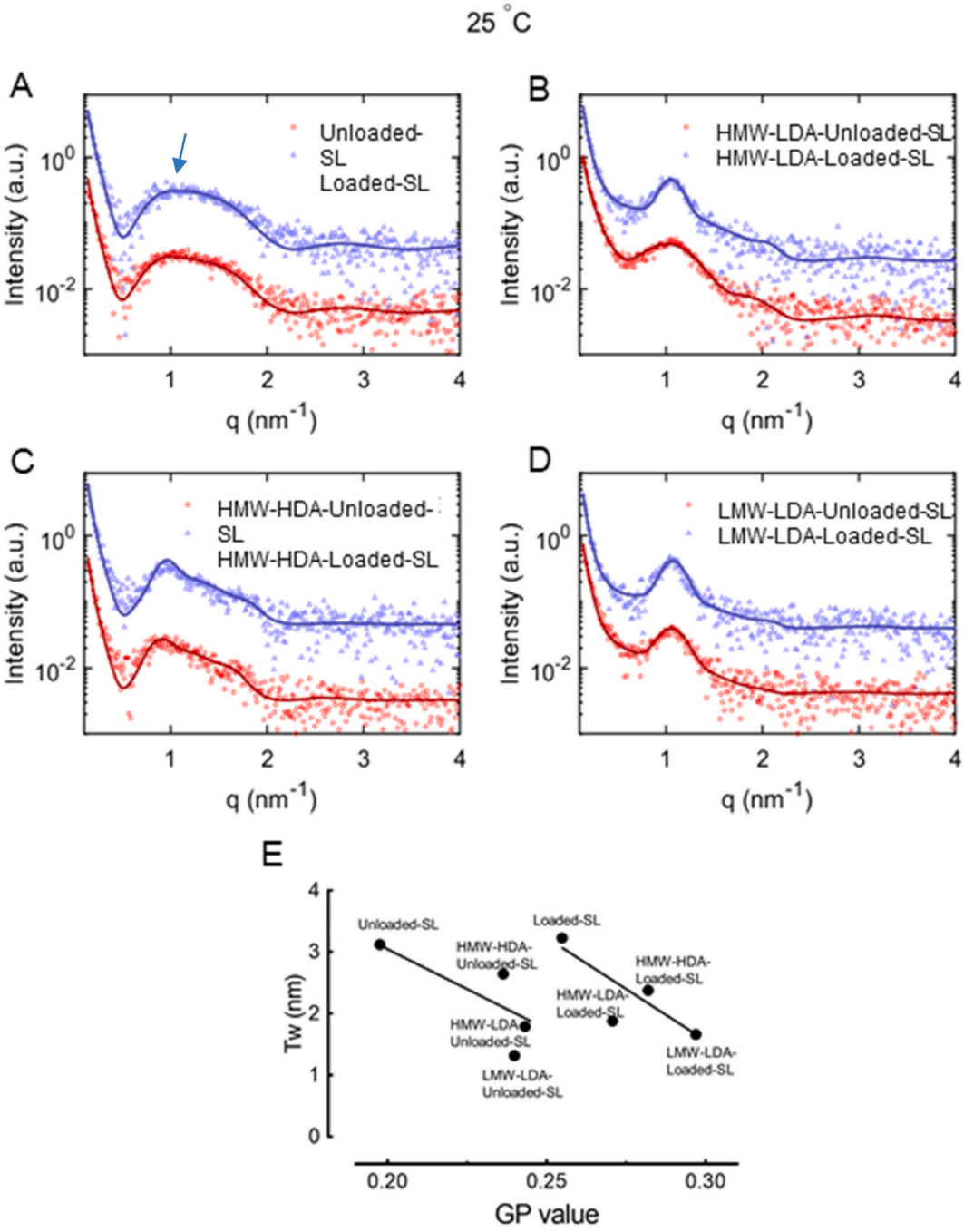

Fig. 4. Variation in background subtracted SAXS intensity scattering as a function of the scattering vector for liposomal formulations loaded with LL17-32 AMP (blue traces) or unloaded (red traces) in 10 mM NaCl at 25 °C and comprised by: (A) SL; (B) HMW-LDA-SL; (C) HMW-HAD-SL; and (D) LMW-LDA-SL. The solid lines represent the global fitting of the experimental data by the global analysis method. (E) Correlation of the generalised polarisation (GP) value of Laurdan fluorescence intensity at 37 °C and the water layer thickness (Tw) for the different liposomes. The plot shows the best-fit linear fit obtained for the data.

different kinds of chitosan-coated liposomes. At this stage, we can only speculate that other phenomena besides chitosan electrostatic binding to the SL membrane are at play. These might involve cooperation and other effects associated with the chitosan structure that influences the membrane fluidity.

SAXS studies of the different liposomal formulations enabled to gain further insight into the membrane structure. Phospholipid-based liposomes unloaded or loaded with LL17-32 peptide were measured in the q range of 0.14–8 nm^{-1} at 25 and 75 °C. The SAXS intensity curves recorded at both temperatures are shown in Fig. 4 and **S8**, respectively. For each system, the data compares the loaded and unloaded formulations. The scattering data were analysed using a global approach that simulates the scattering curves over

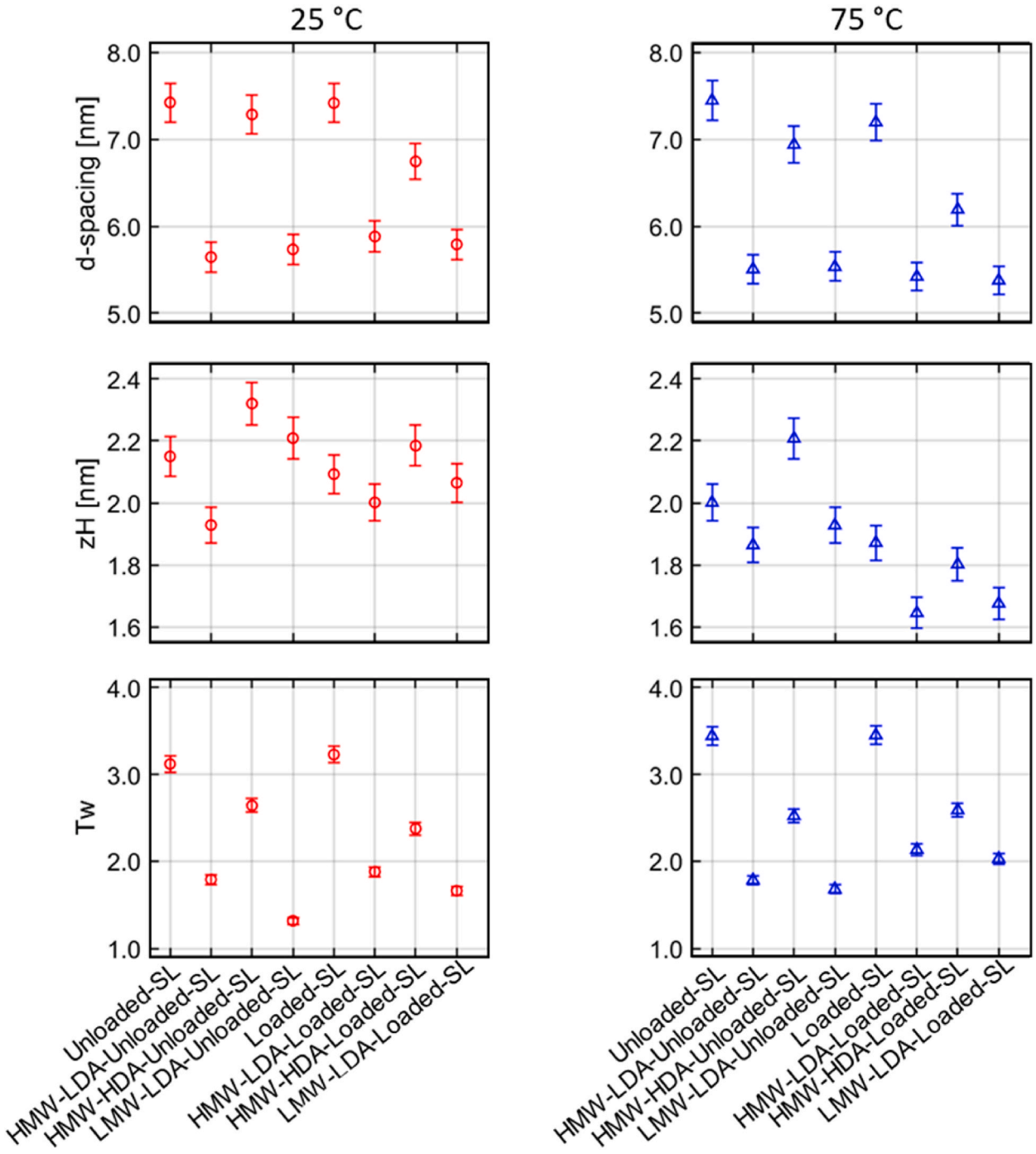

Fig. 5. Comparison of d-spacing, half-bilayer thickness (zH) and the water layer thickness (Tw) data for the different liposomal formulations both unloaded or loaded with LL17-32 peptide, at 25 (left) and 75 °C (right).

the broad range of measured scattering vector magnitude (q) [72](see also methods **Section 2.11**). We note that the scattering intensity was simulated by taking into account both the form factor and the structure factor in the phospholipid lamellar structures. While the former treatment models unilamellar bilayer properties, the latter determines how different lamellae are registered in correlation with each other, comprising the structure of multilamellar vesicles. Noteworthy, the most indicative scattering feature of the structure factor in liquid crystalline lamellar systems is the observation of a distinct Bragg diffraction peak, originating from the constructive interference of diffracted X-ray by equidistant multiple layers. When a low number of layers are registered at equidistant intervals in multilamellar vesicles, the diffraction peak becomes subtle, until disappearing entirely when unilamellar vesicles are formed. Hence, the more the number of layers in multilamellar vesicles, the higher the contribution from the structure factor to the total scattering and the stronger the Bragg diffraction peak intensity. The SAXS profiles of all studied samples demonstrate a distinct diffraction peak at around ~1 nm^{-1}, except the pristine and peptide-loaded SL samples (see panel Fig. 4A and **S8 A**). However, a careful look into their scattering profiles denotes a weak diffraction peak, suggesting that more than one bilayer is in registry. We note that this observation was further confirmed after applying the global analysis approach (see **Section 2.11**), particularly where a unilamellar vesicle model fails to explain the entire X-ray scattering behaviour.

This modelling approach can provide multiple output parameters, aiding in understanding the structure and dynamics of phospholipid membranes. In particular, we focused on the bilayer thickness ($2^{\cdot}$zH), *i.e.*, the distance between two phosphate groups within the phospholipid bilayer cross-section, the *d*-spacing of the multilamellar membranes and the thickness of the interbilayer water region that separates the lamellae (Tw). The global analysis of lipid bilayers also provides a fluctuation parameter of the membranes, which involves the bending modulus of the lipid membrane and its bulk compression modulus [41]. This parameter is often used to assess the membrane fluidity; however, one must consider that its accuracy is highly associated with the mean number of coherent bilayers in the stack. All scattering profiles in our experiments denote only a few (<10) bilayers in correlation due to the extrusion applied during the sample preparation. Such a low number of bilayers led to broad diffraction peaks in the scattering profiles, making it impossible to conclude the fluctuation parameter precisely. As a result, we could only use the form factor parameters (the bilayer and the interbilayer thicknesses) to achieve a conclusive picture of the membrane's structure and fluidity. Unlike the uncertainty in peak broadness, the peak positions could be reliably determined in the scattering profiles and the *d*-spacing could be obtained using Bragg's law. The *d*-spacing data obtained by SAXS (Fig. 5) seems to agree with the thickness of the vesicle membranes imaged by TEM on chitosan-coated LL17-32 peptide-loaded liposomes shown in Fig. S6-S7. However, we could not account for the effect of temperature on the lamellar *d*-spacing. Noteworthy that the *d*-spacing is comprised of two parameters, the membrane bilayer and the separating water layer. Obtaining the bilayer membrane thickness from the global analysis and subtracting it from the corresponding *d*-spacing values provides the thickness of the water layer separating bilayers.

There is a strong correlation between the increase in the water layer thickness and the fluidity of lipid membranes; the thicker the water layer, the higher the membrane fluidity [73]. The high fluidity is observed indirectly by faster and higher vertical motions of bilayers when separated by thicker water layers. Therefore, we considered in our discussion the water layer thickness (or adjacent bilayer distance) as an indirect measure of membrane fluidity.

SL-liposomal membranes demonstrate similar structural properties to their corresponding formulations in the presence of LL17-32 AMP, suggesting a minimal interaction of the peptide with phospholipid bilayers. The structural data obtained from SAXS demonstrate some variations in lipid membranes thickness and the interbilayer separation distance in the presence of chitosan, whereas the degree of acetylation seems to play an essential role in this regard. All chitosan-incorporated formulations show a decrease in interbilayer distances and hence a reduction in membrane fluidity (Figs. 4E and **5**). It is also evident from the SAXS profiles that such a reduction in interbilayer distances is accompanied by more intense diffraction peaks, suggesting reduced vertical motions and high coherence in the bilayer stacks. The most dominant reduction in fluidity was observed when a low degree of acetylation (LDA) chitosan was used. We note that low acetylation is associated with the high charge density along the chitosan polymer chain, increasing its probability of interacting with negatively charged phosphate groups on the surface of bilayers. Therefore, we hypothesize that chitosan chains can induce bridging between the neighbouring bilayers, hence bringing them close to each other and reducing molecules' motions and membrane fluidity. In agreement with this idea, this effect seems to be more pronounced for the more densely charged chitosans (HMW-LDA and LMW-LDA) than for the less densely charged chitosan HMW-HDA (Fig. 5) suggesting a reduced bridging efficacy.

In summary, the results of the Laurdan fluorescence and SAXS of the studied systems have helped us to gain further insight into the fluidity and structure of lipid bilayer membranes of liposomes of various types, either chitosan-coated or pristine, both unloaded and loaded with LL17-32 peptide at two different temperatures, 25 and 75 °C. In all cases, chitosan reduced the membrane fluidity as observed by a negative correlation between GP and water layer thickness (Tw) for both unloaded and peptide-loaded formulations (Fig. 4E). However, the stiffening effect of loading the peptide can only be observed in the increase of the GP values, and not in the decrease in Tw (*cf*. unloaded *vs*. loaded data). Further refinement of these studies and modelling of the obtained electron density profile (EDP) data will be necessary to gain further insight into the properties of these systems. Ultimately, these biophysical studies are expected to help us explain the biological results of antibacterial activity against the dental pathogen *Porphyromonas gingivalis*, addressed in the following sections.

3.6. Association efficacy (AE) and in vitro release in reduced transport fluid (RTF)

The AE of LL17-32 in different liposomes were determined by reversed-phase HPLC method after ultrafiltration. The AE accounted for 100 % of the total LL17-32 in all cases, since no free LL17-32 was detected in the supernatants (Table S2). For the positive control, free LL17-32 was loaded in an ultrafiltration centrifuge tube, and >~95 % of the peptide was detected, thus confirming that there were no artefacts at play that could have been caused by the peptide and the ultrafiltration membrane. The high AE measured for the SL-

liposomes systems can be explained due to the high positive net charge of LL17-32, favouring its interaction with negatively charged SL-liposome membranes via strong electrostatic interactions.

Ron-Doitch *et al.* [50], encapsulated LL-37 in PEGylated liposomes with a lower encapsulation yield (>50 %) than our results on the LL17-32. Another study Reijmar *et al.* [74], using fluorimetric and nano gravimetric methods, showed that LL-37 binds strongly to a wide range of surfaces and results in high loading efficiencies. This has also been explained as the result of the formation of nanostructures called "lipodisks", a flat circular lipid bilayer surrounded by a highly curved rim. Also, it was observed that peptides prefer the highly curved edge of the disks. This provided the first quantitative information about the association of LL-37 with lipid nanoparticles. Boge *et al.* [75], further investigated the use of LL-37 loaded cubosomes, folded lipid bilayers curved in 3D space with interwoven water channels, for delivering cationic amphiphilic peptides. The peptide was considered to be almost entirely encapsulated and uniformly distributed throughout the particles. Although we could not find any reports specifically related to LL17-32 peptide loaded lipid-based nanostructures neither pristine nor polymer-coated, our high LL17-32 AE results suggest that the fragmented peptide has a stronger affinity for the liposome membrane than the longer LL-37 peptide. In fact, removing the N-terminal residues 1–12 and unstructured tail residues 32–37 of LL-37 peptide enhances the peptide stability and improves its interaction with the lipid membrane [76,77]. Consequently, based on our results, we believe that LL17–32 may present a better option for interacting with lipid membranes. Further studies are needed to establish whether LL17-32 and other lipids exhibit high AE as reported here.

An *in vitro* release study was also conducted in reduced transport fluid (RTF) (pH = 7.1 at 37 °C) (Table S2). RTF is a buffered mineral salt solution containing the recuing agent dithiothreitol (DTT) and as such is used as an incubation medium in the peptide-induced bacteria-killing essay subject of section below. As shown in Table S2, LL17-32 peptide had not been released from any of the systems for at least 4 h, which could be explained as the consequence of the strong interactions between liposome and peptide. For the positive control, free LL17-32 peptide was loaded in the same dialysis tube and >~90 % of it was recovered, thus ruling out any binding effect of the peptide and the dialysis tube membrane. This result is in agreement with previous studies on LL-37 peptide released from cubosomes, as determined by 24-h dialysis and a fluorescamine assay, that found almost no release due to the tight binding of the peptide to the cubosomes [75]. However, an earlier study by the same group illustrated that in the pure water solution, LL-37 post-loaded cubosomes showed a rapid and high release of close to 100 % over 24 h. It was discovered that the low ionic strength of the buffer and the co-polymeric stabiliser (P407) present in the cubosome samples increased the release of LL-37 across the dialysis membrane [78]. Also, they demonstrated that at the greater ionic strength (150 mM NaCl), the peptide released from the cubosomes was significantly diminished. There is no such release study related to LL17-32 loaded lipid-based structures.

Our results suggest that there was no release of LL17-32 from the system. Based on this phenomenon, we can anticipate that the killing effect of loaded liposomes on bacteria described below is not likely to be dependent on the peptide payload released from the system but is dominated by the particle-bacteria cell interactions.

3.7. Colloidal stability in RTF

The stability of liposomes in RTF was studied from the evolution of the particle size distribution as probed by DLS at varying time intervals up to 240 min at 37 °C. As shown in Fig. 6, LL17-32-loaded and unloaded pristine SL liposomes revealed that these systems remained stable. However, the particle size of both the LMW- and HMW-LDA chitosan-coated liposome formulations (unloaded and loaded) increased by more than an order of magnitude and sediment formation was noticed after ~ 1 h. This increase in size suggests that the high charge density chitosans began to lose their positive charges at a pH higher than their intrinsic pK_o (~6.1, [79]). This loss of positive charges likely led to the aggregation of chitosan-coated liposomes. The data collection for these samples was consequently halted after 60 min. By contrast, the size of HMW-HDA chitosan-coated liposomes showed only a slight increase after ~30 min followed by a steady decrease to the original size over, diagnostic of colloidal stability over the course of the incubation time.

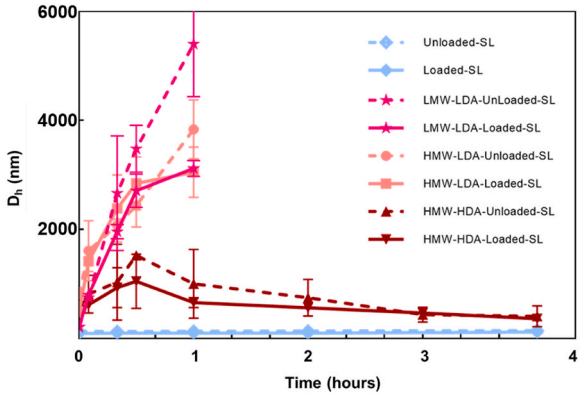

Fig. 6. Evolution of the particle size growth at varying time intervals up to 4 h incubated in RTF medium (pH = 7.1 at 37 °C). All liposome formulations of various types of chitosan (4 mg/mL) coated, uncoated loaded-SL were loaded with 0.6 mg/mL LL17-32. Values are presented as means ± SD (n = 3).

We can argue that HMW-HDA chitosan presents a high surface hydrophilicity. This is probably due to the interaction between the polymer and the liposome's surface, driven not only by electrostatic but also by hydrophobic forces involving the chitosan's GlcNac (A) residues and the alkyl chain of phospholipids (Fig. 7). This hydrophobic force might prevent HDA chitosan disassociating from the liposome surface, thus resulting in better hydrophilicity and colloidal stability of the system. This suggestion agrees well with the explanation of results obtained in chitosan-coated capsaicin nanocapsules comprised of SL oil/water nanoemulsions [58]. In addition to the DLVO theory and steric hindrance, the surrounding ions, also known as coupling ions, play an essential role in determining the colloidal stability and electrokinetic behaviour of particles [80]. These ions generate short-range repulsive hydration forces that arise from the interactions between the charged surfaces of particles and the surrounding water molecules. These hydration forces prevent particles from coming into close contact with one another, which, in turn, affects their stability. The extent of these hydration forces depends on several factors, including the solution pH, nature and concentration of the ions surrounding the surface. In particular, calcium (Ca^{2+}) or magnesium (Mg^{2+}) ions are known to exert a higher restabilization effect compared to sodium (Na^{+}) ions due to their greater ability to generate repulsion mediated by hydration forces. This phenomenon is attributed to the higher hydration energy of divalent cations, which leads to a more extensive hydration shell around the ion.

3.8. Bactericidal activity against Porphyromonas gingivalis

The potential killing activities of peptide LL17-32, LL17-32 associated particles, and free chitosans against *P. gingivalis* were investigated (Fig. 8). As an obligate anaerobe, *P. gingivalis* must be grown under anaerobic conditions and forms black colonies on blood agar (Fig. S9) and was quantified by viable counts. The free form antimicrobial peptide LL17-32 displayed promising and rapid killing effects on *P. gingivalis*. A significant reduction to approximately 10 % of viable counts (as normalised to control) was seen at a concentration of 3.75 μg/mL, this continued in a dose dependant manner till no colonies were detected at 30 μg/mL (Fig. 8A). The proteolytic pathogen *P. gingivalis* is involved in the degradation of extracellular matrix proteins via the activity of the secreted endopeptidase enzymes Arg-gingipain (Rgp) and Lys-gingipain (Kgp) [81]. LL-37 was also found in a degraded form at sites in which *P. gingivalis* was shown to be present at high levels [14]. Devine *et al.* [15], isolated extracellular proteases of *P. gingivalis*, and demonstrated they strongly inactivated a range of antimicrobial peptides ranging in size from 14 to 36 amino acids. Theoretically, peptide LL17-32 is susceptible to gingipain-mediated protease inactivation through specific cleavage at Lys and Arg residues within its amino acid sequence. Paradoxically, despite the possibility that LL17-32 would be susceptible to gingipain-mediated degradation, our

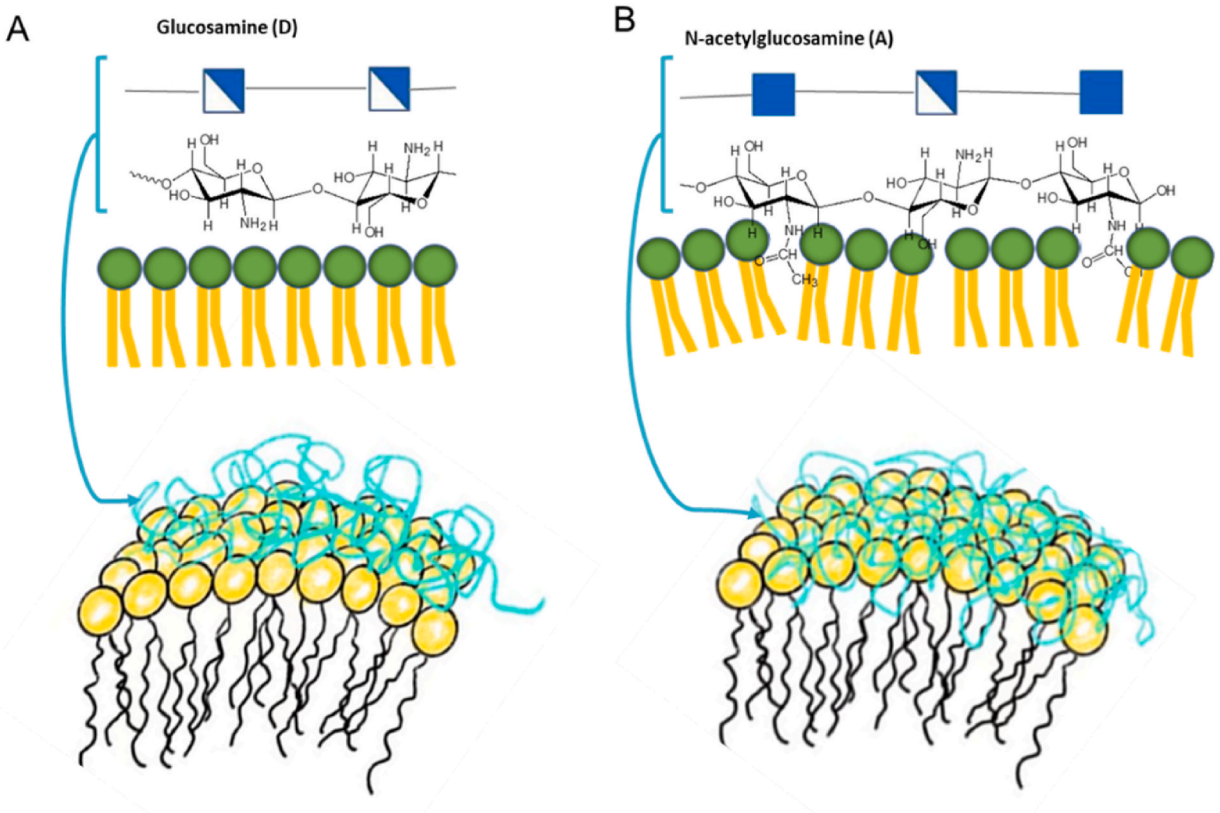

Fig. 7. Schematic models for the interaction between chitosan and lipid membrane at the phospholipidic surface for chitosans of (A) LDA (low degree of acetylation); (B) HDA (high degree of acetylation).

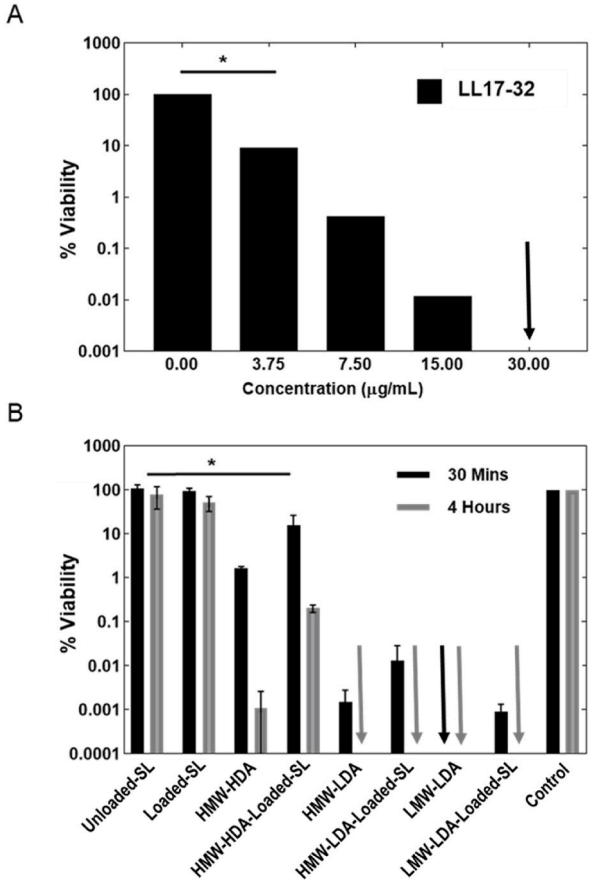

Fig. 8. Susceptibility to killing *P. gingivalis* cells grown at 37 °C. Effects of peptide LL17-32 at different concentrations on the bacterial cell viability (30 min) (A); Effects of three types of chitosans (free form) and chitosan-coated/uncoated liposomal LL17-32-loaded formulations on the bacterial cell viability (B). Cell viability was determined as a percentage of cell viability relative to an untreated control corresponding to 100 % viability colony counts and presented as means ± SD ($n = 3$). Pairwise Student's t-test statistical comparisons between the Loaded-SL, HMW- HDA, and HMW- HDA-Loaded-SL, with Unloaded-SL at 30 min (*$p < 0.05$). All chitosan-coated formulations (at 4 mg/mL) and pristine (Loaded-SL) were loaded with 0.6 mg/mL LL17-32. In each 96 microplates well, the concentration of various chitosan and peptide LL17-32 were 0.2 mg/mL and 30 μg/mL, respectively. ↓ Symbols denote cell viability values below the minimum detection limit of 0.000001 % with respect to control.

results showed that its ability to kill *P. gingivalis* was not attenuated in these studies. A possible assumption is that the disruption of bacteria membrane by peptide occurred more rapidly than the total degradation of the peptide by proteases. Cecropin B, an antimicrobial peptide that includes two alpha helix structures, was inactivated very slowly (10–15 min) by *P. gingivalis* proteases [15]. However, there is no such study relating to the protease-mediated inactivation of LL17-32. Another possible reason is due to the abundance of Arg-gingipain (Rgp) and Lys-gingipain (Kgp) depletion during the washing step using RTF.

Chitosan is well known for its antimicrobial activity against a wide range of microorganisms. The precise mechanisms of chitosan in killing and inhibiting the growth of bacteria are complex and not fully elucidated. The most likely mechanism is electrostatic interactions between cations R–N $(CH_3)^+$ in chitosan backbone and anionic bacteria cell wall constituents such as lipopolysaccharide and phospholipids. This strong ionic interaction disrupts the bacteria membrane and alters the membrane permeability, resulting in an imbalanced osmotic pressure and ion exchange. This triggers the leakage of intracellular material and cell lysis, resulting in bacteria death [82–84]. Chitosan could also form complexes with surrounding ions due to its trace metal chelating ability, which alters bacteria's metabolic function leading to bacterial death [85]. Furthermore, certain sizes of chitosan can penetrate through the nuclei of microorganisms and bind with DNA to interfere with mRNA and the process of protein synthesis [86]. The killing activities of chitosan with different DA and Mw against *P. gingivalis* are presented in Fig. 8B. For a similar degree of acetylation, LMW-LDA chitosan presented a greater killing effect compared to HMW-LDA chitosan.

Contradictory results regarding the antimicrobial activity of chitosan against *P.gingivalis* have previously been reported. Ikinci *et al.* [87], examined high Mw chitosan (Mw~1400 kDa) and demonstrated greater antimicrobial activities against *P. gingivalis* than low Mw chitosan (Mw~272 kDa). On the other hand, Costa et al. [88], reported *P. gingivalis* showed similar minimum inhibitory concentrations (MIC) values for both HMW and LMW chitosans. These discrepant results could be due to the proportional differences in Mw, specifically, ~624 and ~107 kDa chitosan were used as HMW and LMW, respectively, in the aforementioned study, whereas chitosans of

~106 kDa (HMW) and ~39 kDa (LMW) were studied in this project, both of similar low degree of acetylation (DA = 15–16%). Also, different strains of *P. gingivalis* have been used in each study. In addition to the Mw of chitosan, the degree of acetylation also influences the antimicrobial effect of chitosan [89–91]. HMW-LDA chitosan killed *P. gingivalis* more rapidly than HMW-HDA chitosan, which is possibly due to the higher amount of protonated glucosamine groups in LDA chitosan resulting in high charge density. This leads to a stronger electrostatic interaction between the chitosan backbone and bacteria surface, resulting in bacterial death. In their study, Chen *et al.* [92] investigated the antimicrobial ability of chitosans of three different DAs against six-bacterial pathogens. It was suggested that chitosan with LDA exhibited a higher antimicrobial ability. It is worth mentioning that the antibacterial activity of chitosan is also critically reliant on the pH of the assay buffer since at pH > ~6.1 [79] chitosan can lose its positive charge and precipitate out of the solution. The majority of *in vitro* studies [87,88,93,94] have neglected to address the pH change, given that chitosan is commonly dissolved in acetic acid, which could alter the pH and final findings related to its antimicrobial ability.

The three kinds of chitosan-coated liposomal LL17-32 systems tested, presented slower and less effective killing activity against *P. gingivalis* than free chitosans in solution. Particularly the HMW-HDA-Loaded-SL sample elicited slower but sustained killing. This result correlated with the previous discovery of physical stability in RTF (Fig. 6), for which we hypothesized the hydrophobic force between chitosan and phospholipids was the mechanism slowing the rate of polymer dissociation from the liposomal surface. Unexpectedly, the liposomal formulation loaded-SL devoid of chitosan coating did not show any discernible bacterial killing effects. This suggests that chitosan and, not the delivery of LL17-32 payload, is responsible for the killing effect observed in all chitosan-coated SL liposomes. This proposal is supported by the result that the LL17-32 peptide did not release from the SL liposome in the RTF buffer and, thereby, could not exert its bactericidal effect. Furthermore, as described in **Section 3.3**, the LL17-32 loaded-SL liposomal formulation has a negative overall surface charge (indicated by a negative ζ-potential), which creates an electrostatic repulsive force between the negatively charged SL liposomes and the negatively charged surface of *P. gingivalis*. Thus, electrostatic-driven adhesion or fusion of liposomes to the bacteria would be disfavoured. Even when LL17-32-loaded, neither chitosan-coated nor pristine SL-liposomes showed greater bactericidal activity than the free peptide, we venture to suggest that in the *in vivo* physiological context, in the presence of abundant human and bacterial enzymes (*e.g.* lingual lipase, lysosome, chitosanases), the situation might be very different, and LL17-32 could be released to display its bactericidal effect. To address to some extent the validity of this proposal, as a preliminary test, RTF (free of enzymes) was replaced by sterilised saliva (Fig. S9), and the bactericidal effect of a selected chitosan-coated (HMW-HDA-Loaded-SL) and pristine (Loaded-SL) liposomal formulations, and the free peptide and chitosan, on *P. gingivalis* cell viability was examined. Almost no such activity was observed for the Loaded-SL liposome formulation, which suggested that LL17-32 seemed not to be released from the SL liposome (Fig. S9). Additionally, the bactericidal activity against *P. gingivalis* of free LL17-32, chitosan, and chitosan-coated SL liposome in saliva were all attenuated. This is possibly due to the ionic strength and presence of enzymes in physiological conditions which affect the function of peptides and chitosan [95,96]. This would be an interesting area to investigate more thoroughly in the future studies.

4. Conclusion

The use of small colloidal particles as carriers of bioactive molecules with poor bioavailability to enable them to overcome physical and biological barriers and enhance their therapeutic efficacy is a priority of biomedical research and development, including the dental sector. In this work, we investigated the loading of the antimicrobial peptide fragment LL17-32 in liposomal formulations comprised by soya lecithin phospholipids either pristine or coated with chitosans of varying Mw and DA. All formulations were found to invariably associate the peptide with high efficiency (>95 %). This high association efficiency resulted in a negligible *in vitro* release of the payload in biologically relevant conditions. Chitosan-coated LL17-32 loaded/unloaded liposomes exhibited increased size and a positive ζ-potential, reversed from the negatively charged pristine SL-liposomes. The Mw of chitosan had a substantial impact on the particle size. As expected, high Mw chitosan-coated liposomes presented larger particle sizes. The high DA (HDA)chitosan-coated systems showed better colloidal stability compared to those comprised of low DA (LDA)-chitosans. In general, coating with chitosan and peptide LL17-32 loading significantly decreased the fluidity of liposome membranes when compared with the surface-pristine unloaded SL-liposome. For the biological studies, peptide LL17-32 and free chitosans all demonstrated strong bactericidal effects against *P. gingivalis*. Especially LMW-LDA chitosan, bearing a more densely positive charge and killed the bacteria more quickly. However, for LL17-32 loaded SL-liposomes, this killing effect was dramatically attenuated. Also, for three chitosan-coated LL17-32 loaded SL-liposome systems, the bacterial killing effects decreased. Chitosans alone, not LL17-32, may be responsible for the observed antibacterial activity in all chitosan-coated LL17-32 loaded SL liposomes. The results of the present study have significant implications for understanding the considerations in the initial development stages of liposome and chitosan-based nanomaterials for potential delivery of antimicrobial peptide LL17-32 in dental applications.

CRediT authorship contribution statement

Jinyang Han: Writing – review & editing, Writing – original draft, Methodology, Investigation, Formal analysis. **Josephine Meade:** Writing – review & editing, Supervision, Investigation, Conceptualization. **Deirdre Devine:** Writing – review & editing, Supervision, Conceptualization. **Amin Sadeghpour:** Writing – review & editing, Formal analysis, Data curation. **Michael Rappolt:** Writing – review & editing, Validation, Data curation, Conceptualization. **Francisco M. Goycoolea:** Writing – review & editing, Supervision, Project administration, Investigation, Conceptualization.

Declaration of competing interest

The authors declare the following financial interests/personal relationships which may be considered as potential competing interests: Francisco M. Goycoolea reports equipment, drugs, or supplies was provided by Diamond Light Source Ltd. If there are other authors, they declare that they have no known competing financial interests or personal relationships that could have appeared to influence the work reported in this paper.

Acknowledgements

We are grateful to Dr. Joanne Maycock and Dr. Dr Sam Burholt, for their expert advice and support in the execution of this work. Beam time access to DL-SAXS at Diamond Light Source LTd (UK) and support from the School of Food Science and Nutrition of University of Leeds are gratefully acknowledged.

Appendix A. Supplementary data

Supplementary data to this article can be found online at https://doi.org/10.1016/j.heliyon.2024.e34554.

References

[1] P.E. Petersen, H. Ogawa, The global burden of periodontal disease: towards integration with chronic disease prevention and control, Periodontol. 2000 60 (2012) 15–39.
[2] A. Hugoson, B. Sjodin, O. Norderyd, Trends over 30 years, 1973-2003, in the prevalence and severity of periodontal disease, J. Clin. Periodontol. 35 (2008) 405–414.
[3] I. Olsen, J.D. Lambris, G. Hajishengallis, Porphyromonas gingivalis disturbs host-commensal homeostasis by changing complement function, J. Oral Microbiol. 9 (2017) 1340085.
[4] G. Hajishengallis, et al., Low-abundance biofilm species orchestrates inflammatory periodontal disease through the commensal microbiota and complement, Cell Host Microbe 10 (2011) 497–506.
[5] G. Hajishengallis, Periodontitis: from microbial immune subversion to systemic inflammation, Nat. Rev. Immunol. 15 (2015) 30–44.
[6] R.P. Darveau, G. Hajishengallis, M.A. Curtis, Porphyromonas gingivalis as a potential community activist for disease, J. Dent. Res. 91 (2012) 816–820.
[7] F.A.F. Oliveira, et al., Molecular analysis of oral bacteria in heart Valve of patients with cardiovascular disease by real-time polymerase chain reaction, Medicine (Baltim.) 94 (2015) e2067.
[8] K.J. Maresz, et al., Porphyromonas gingivalis facilitates the development and progression of destructive arthritis through its unique bacterial peptidylarginine deiminase (PAD), PLoS Pathog. 9 (2013) e1003627.
[9] P.S. Kumar, From focal sepsis to periodontal medicine: a century of exploring the role of the oral microbiome in systemic disease, J. Physiol. 595 (2017) 465–476.
[10] J. Gnanasekaran, et al., Intracellular Porphyromonas gingivalis promotes the tumorigenic behavior of pancreatic carcinoma cells, Cancers 12 (2020).
[11] S.S. Dominy, et al., Porphyromonas gingivalis in Alzheimer's disease brains: evidence for disease causation and treatment with small-molecule inhibitors, Sci. Adv. 5 (2019) eaau3333.
[12] J.M. Conlon, et al., A family of antimicrobial and immunomodulatory peptides related to the frenatins from skin secretions of the Orinoco lime frog Sphaenorhynchus lacteus (Hylidae), Peptides 56 (2014) 132–140.
[13] A.A. Bahar, D. Ren, Antimicrobial peptides, Pharmaceuticals 6 (2013) 1543–1575.
[14] Y. Takeuchi, et al., Salivary levels of antibacterial peptide (LL-37/hCAP-18) and cotinine in patients with chronic periodontitis, J. Periodontol. 83 (2012) 766–772.
[15] D.A. Devine, et al., Modulation of antibacterial peptide activity by the product of p.gingivalis and Prevotella spp, Microbiology 145 (1999) 965–971.
[16] L. Grassi, et al., Combination strategies to enhance the efficacy of antimicrobial peptides against bacterial biofilms, Front. Microbiol. 8 (2017) 2409.
[17] X. Li, et al., Solution structures of human LL-37 fragments and NMR-based identification of a minimal membrane-targeting antimicrobial and anticancer region, J. Am. Chem. Soc. 128 (2006) 5776–5785.
[18] A. de Miguel Catalina, et al., The C-terminal VPRTES tail of LL-37 influences the mode of attachment to a lipid bilayer and antimicrobial activity, Biochemistry 58 (2019) 2447–2462.
[19] A.D. Bangham, M.M. Standish, J.C. Watkins, Diffusion of univalent ions across the lamellae of swollen phospholipids, J. Mol. Biol. 13 (1965), 238-IN27.
[20] M. Hasan, et al., Synthesis of loureirin B-loaded nanoliposomes for pharmacokinetics in rat plasma, ACS Omega 4 (2019) 6914–6922.
[21] M. Hasan, I. Javed, Umer Awan, Nian Xin, Hao Dang, Baradi Waryani, Yasmeen Saeed, Kaleem Ullah, Dai Rongji, Yulin Deng, LX loaded nanoliposomes synthesis, characterization and cellular uptake studies in H2O2 stressed SH-SY5Y cells, J. Nanosci. Nanotechnol. 14 (2014) 4066–4071.
[22] A. Akbarzadeh, et al., Liposome: classification, preparation, and applications, Nanoscale Res. Lett. 8 (2013) 1–9.
[23] V. Andra, et al., A comprehensive review on novel liposomal methodologies, commercial formulations, clinical trials and patents, Bionanoscience 12 (2022) 274–291.
[24] K. Gradauer, et al., Chemical coupling of thiolated chitosan to preformed liposomes improves mucoadhesive properties, Int. J. Nanomed. 7 (2012) 2523–2534.
[25] M. Werle, H. Takeuchi, Chitosan-aprotinin coated liposomes for oral peptide delivery: development, characterisation and in vivo evaluation, Int. J. Pharm. 370 (2009) 26–32.
[26] H. Sugihara, et al., Effectiveness of submicronized chitosan-coated liposomes in oral absorption of indomethacin, J. Liposome Res. 22 (2012) 72–79.
[27] H. Takeuchi, et al., Enteral absorption of insulin in rats from mucoadhesive chitosan-coated liposomes, Pharmaceut. Res. 13 (1996) 896–901.
[28] K. Tai, et al., The stabilization and release performances of curcumin-loaded liposomes coated by high and low molecular weight chitosan, Food Hydrocolloids 99 (2020).
[29] T. Mengoni, et al., A chitosan-based liposome formulation enhances the in vitro wound healing efficacy of substance P neuropeptide, Pharmaceutics 9 (2017).
[30] P. Artursson, et al., Effect of chitosan on the permeability of monolayers of intestinal epithelial cells (Caco-2), Pharmaceut. Res. 11 (1994) 1358–1361.
[31] H. He, et al., Adapting liposomes for oral drug delivery, Acta Pharm. Sin. B 9 (2019) 36–48.
[32] J. Kowapradit, et al., Methylated N-(4-N,N-dimethylaminobenzyl) chitosan coated liposomes for oral protein drug delivery, Eur. J. Pharmaceut. Sci. 47 (2012) 359–366.
[33] S.D. O'Neill, A.C.P.P. Leopold, An assessment of phase transitions in soybean membranes, Plant Physiol. 70 (1982) 1405–1409.
[34] D. Marsh, Thermodynamics of phospholipid self-assembly, Biophys. J. 102 (2012) 1079–1087.

[35] G. Weber, F.J. Farris, Synthesis and spectral properties of a hydrophobic fluorescent probe: 6-propionyl-2-(dimethylamino) naphthalene, Biochemistry 18 (1979) 3075–3078.
[36] H.J. Kaiser, et al., Order of lipid phases in model and plasma membranes, Proc. Natl. Acad. Sci. U.S.A. 106 (2009) 16645–16650.
[37] A. Sadeghpour, et al., Comparative study of interactions of aliskiren and AT1 receptor antagonists with lipid bilayers, Biochim. Biophys. Acta Biomembr. 1848 (2015) 984–994.
[38] B. Drasler, et al., Fullerene up-take alters bilayer structure and elasticity: a small angle X-ray study, Chem. Phys. Lipids 188 (2015) 46–53.
[39] D. Sanver, et al., Experimental modeling of flavonoid–biomembrane interactions, Langmuir 32 (2016) 13234–13243.
[40] D. Sanver, et al., Structure and dynamics of dioleoyl-phosphatidylcholine bilayers under the influence of quercetin and rutin, Langmuir 36 (2020) 11776–11786.
[41] G. Pabst, et al., Structural information from multilamellar liposomes at full hydration: full q-range fitting with high quality x-ray data, Phys. Rev. 62 (2000) 4000–4009.
[42] M. Rappolt, P. Laggner, G. Pabst, Structure and elasticity of phospholipid bilayers in the Lα phase: a comparison of phosphatidylcholine and phosphatidylethanolamine membranes, in: S.G. Pandalai (Ed.), Recent Research Developments in Biophysics, Transworld Research Network, Trivandrum, 2004, pp. 365–394.
[43] A. Caillé, Remarques sur la diffusion des rayons X dans les smectiques. C R Acad Sci Serie 5 274 (1972) 891–893.
[44] M.A. Curtis, et al., Temperature-dependent modulation ofPorphyromonas gingivalisLipid A structure and interaction with the innate host defenses, Infect. Immun. 79 (2011) 1187–1193.
[45] S.H. Bang, et al., Influence of chitosan coating on the liposomal surface on physicochemical properties and the release profile of nanocarrier systems, J. Microencapsul. 28 (2011) 595–604.
[46] S.H. Bang, et al., Formation of size-controlled nano carrier systems by self-assembly, J. Microencapsul. 26 (2009) 722–733.
[47] C. Tan, et al., Dual effects of chitosan decoration on the liposomal membrane physicochemical properties as affected by chitosan concentration and molecular conformation, J. Agric. Food Chem. 61 (2013) 6901–6910.
[48] J.E. Nielsen, et al., Beyond structural models for the mode of action: how natural antimicrobial peptides affect lipid transport, J. Colloid Interface Sci. 582 (2021) 793–802.
[49] E. Sevcsik, et al., How lipids influence the mode of action of membrane-active peptides, Biochim. Biophys. Acta 1768 (2007) 2586–2595.
[50] S. Ron-Doitch, et al., Reduced cytotoxicity and enhanced bioactivity of cationic antimicrobial peptides liposomes in cell cultures and 3D epidermis model against HSV, J. Contr. Release 229 (2016) 163–171.
[51] L.M. Were, et al., Size, stability, and entrapment efficiency of phospholipids nanocapsules containing polypeptide antimicrobials, J. Agric. Food Chem. 51 (2003) 8073–8079.
[52] S. Afonin, et al., Temperature-dependent transmembrane insertion of the amphiphilic peptide PGLa in lipid bilayers observed by solid state 19F NMR spectroscopy, J. Am. Chem. Soc. 130 (2008) 16512–16514.
[53] J. Burck, et al., Conformation and membrane orientation of amphiphilic helical peptides by oriented circular dichroism, Biophys. J. 95 (2008) 3872–3881.
[54] R.W. Glaser, et al., Concentration-dependent realignment of the antimicrobial peptide PGLa in lipid membranes observed by solid-state 19F-NMR, Biophys. J. 88 (2005) 3392–3397.
[55] D. Rapaport, et al., pH-and ionic strength-dependent fusion of phospholipid vesicles induced by pardaxin analogs or by mixtures of charge-reversed peptides, Biochemistry 32 (1993) 3291–3297.
[56] P. Tremouilhac, et al., Conditions affecting the re-alignment of the antimicrobial peptide PGLa in membranes as monitored by solid state 2H-NMR, Biochim. Biophys. Acta 1758 (2006) 1330–1342.
[57] Z. Li, A.T. Paulson, T.A. Gill, Encapsulation of bioactive salmon protein hydrolysates with chitosan-coated liposomes, J. Funct.Foods 19 (2015) 733–743.
[58] F.M. Goycoolea, et al., Chitosan-based nanocapsules: physical characterization, stability in biological media and capsaicin encapsulation, Colloid Polym. Sci. 290 (2012) 1423–1434.
[59] U. Klinkesorn, et al., Encapsulation of emulsified tuna oil in two-layered interfacial membranes prepared using electrostatic layer-by-layer deposition, Food Hydrocolloids 19 (2005) 1044–1053.
[60] C. Laye, D.J. McClements, J. Weiss, Formation of biopolymer-coated liposomes by electrostatic deposition of chitosan, J. Food Sci. 73 (2008) N7–N15.
[61] G. Sandri, Assessment of chitosan derivatives as buccal and vaginal penetration enhancers, Eur. J. Pharmaceut. Sci. 21 (2004) 351–359.
[62] D.O. Shah, Interaction of uranyl ions with phospholipid and cholesterol monolayers, J. Colloid Interface Sci. 29 (1969) 210–215.
[63] H.L. Scott, et al., On the mechanism of bilayer separation by extrusion, or why your LUVs are not really unilamellar, Biophys. J. 117 (2019) 1381–1386.
[64] A. Ghadi, et al., Synthesis and optimization of chitosan nanoparticles: potential applications in nanomedicine and biomedical engineering, Caspian Journal of Internal Medicine 5 (2014) 156.
[65] M. Schaechter, Encyclopedia of Microbiology, Academic Press., 2009.
[66] D.A. Los, N. Murata, Membrane fluidity and its roles in the perception of environmental signals, Biochim. Biophys. Acta 1666 (2004) 142–157.
[67] B. Ladbrooke, D. Chapman, Thermal analysis of lipids, proteins and biological membranes a review and summary of some recent studies, Chem. Phys. Lipids 3 (1969) 304–356.
[68] F.M. Harris, K.B. Best, J.D. Bell, Use of laurdan fluorescence intensity and polarization to distinguish between changes in membrane fluidity and phospholipid order, Biochim. Biophys. Acta Biomembr. 1565 (2002) 123–128.
[69] S.L. Veatch, et al., Critical fluctuations in domain-forming lipid mixtures, Proc. Natl. Acad. Sci. USA 104 (2007) 17650–17655.
[70] A. Morales-Martinez, et al., Membrane fluidity, composition, and charge affect the activity and selectivity of the AMP ascaphin-8, Biophys. J. 121 (2022) 3034–3048.
[71] C. Tan, et al., Biopolymer-coated liposomes by electrostatic adsorption of chitosan (chitosomes) as novel delivery systems for carotenoids, Food Hydrocolloids 52 (2016) 774–784.
[72] G. Pabst, Global properties of biomimetic membranes: perspectives on molecular features, Biophys.Rev.Letters 1 (2006) 57–84.
[73] G. Pabst, et al., Structural analysis of weakly ordered membrane stacks, J. Appl. Crystallogr. 63 (2003) 1378–1388.
[74] K. Reijmar, et al., Characterizing and controlling the loading and release of cationic amphiphilic peptides onto and from PEG-stabilized lipodisks, Langmuir 32 (2016) 12091–12099.
[75] L. Boge, et al., Cubosomes for topical delivery of the antimicrobial peptide LL-37, Eur. J. Pharm. Biopharm. 134 (2019) 60–67.
[76] K. Bandurska, et al., Unique features of human cathelicidin LL-37, Biofactors 41 (2015) 289–300.
[77] M. Wanmakok, et al., Expression in Escherichia coli of novel recombinant hybrid antimicrobial peptide AL32-P113 with enhanced antimicrobial activity in vitro, Gene 671 (2018) 1–9.
[78] L. Boge, et al., Cubosomes post-loaded with antimicrobial peptides: characterization, bactericidal effect and proteolytic stability, Int. J. Pharm. 526 (2017) 400–412.
[79] M. Rinaudo, G. Pavlov, J. Desbrieres, Solubilization of chitosan in strong acid medium, Int. J. Polym. Anal. Char. 5 (1999) 267–276.
[80] M.J. Santander-Ortega, et al., Chitosan nanocapsules: effect of chitosan molecular weight and acetylation degree on electrokinetic behaviour and colloidal stability, Colloids Surf. B Biointerfaces 82 (2011) 571–580.
[81] K.Y. How, K.P. Song, K.G. Chan, Porphyromonas gingivalis: an overview of periodontopathic pathogen below the gum line, Front. Microbiol. 7 (2016) 53.
[82] H. Seo, et al., Antibacterial fiber blended with chitosan, in: Chitin World, Wirtschaftverlag, Germany, 1994, pp. 623–631.
[83] F. Kara, et al., Synthesis and surface modification of polyurethanes with chitosan for antibacterial properties, Carbohydr. Polym. 112 (2014) 39–47.
[84] J. Li, Y. Wu, L. Zhao, Antibacterial activity and mechanism of chitosan with ultra high molecular weight, Carbohydr. Polym. 148 (2016) 200–205.
[85] Z. Jia, W. Xu, Synthesis and antibacterial activities of quaternary ammonium salt of chitosan, Carbohydr. Res. 333 (2001) 1–6.
[86] E.I. Rabea, et al., Chitosan as antimicrobial agent: applications and mode of action, Biomacromolecules 4 (2003) 1457–1465.

[87] G. Ikinci, et al., Effect of chitosan on a periodontal pathogen Porphyromonas gingivalis, Int. J. Pharm. 235 (2002) 121–127.
[88] E.M. Costa, et al., Evaluation and insights into chitosan antimicrobial activity against anaerobic oral pathogens, Anaerobe 18 (2012) 305–309.
[89] S. Tokura, et al., Molecular weight dependent antimicrobial activity by chitosan, in: New Macromolecular Architecture and Functions, Springer, Berlin, Heidelberg, 1996, pp. 199–207.
[90] K. Shibasaki, et al., Effects of low molecular chitosan on pH changes in human dental plaque, Bull. Tokyo Dent. Coll. 35 (1994) 33–39.
[91] X. Qin, J. Emich, F.M. Goycoolea, Assessment of the quorum sensing inhibition activity of a non-toxic chitosan in an N-acyl homoserine lactone (AHL)-Based Escherichia coli biosensor, Biomolecules 8 (2018).
[92] Y.M. Chen, et al., Antibacterial properties of chitosan in waterborne pathogen, Journal of Environmental Science and Health 37 (2002) 1379–1390.
[93] D.D. Divakar, et al., Enhanced antimicrobial activity of naturally derived bioactive molecule chitosan conjugated silver nanoparticle against dental implant pathogens, Int. J. Biol. Macromol. 108 (2018) 790–797.
[94] L. Mooduto, D.A. Wahjuningrum, C.G. Lunardhi, Antibacterial effect of chitosan from squid pens against Porphyromonas gingivalis bacteria, Iran. J. Microbiol. 11 (2019) 177.
[95] W.F. Walkenhorst, Using adjuvants and environmental factors to modulate the activity of antimicrobial peptides, Biochim. Biophys. Acta 1858 (2016) 926–935.
[96] C.A. Marangon, et al., The effects of ionic strength and pH on antibacterial activity of hybrid biosurfactant-biopolymer nanoparticles, J. Appl. Polym. Sci. 139 (2021).